Liao *et al. Chem Synth* 2024;4:18
DOI: 10.20517/cs.2023.47

Chemical Synthesis

Review

Open Access

The emerging Sr_2FeMoO_6-based electrocatalysts for solid oxide electrochemical cell: synthesis, modulation and applications

Yuanfeng Liao, Xiuan Xi, Hao Chen, Jianwen Liu*, Xian-Zhu Fu, Jing-Li Luo*

Shenzhen Key Laboratory of Energy Electrocatalytic Materials, Guangdong Provincial Key Laboratory of New Energy Materials Service Safety, College of Materials Science and Engineering, Shenzhen University, Shenzhen 518060, Guangdong, China.

***Correspondence to:** Prof. Jing-Li Luo, Dr. Jianwen Liu, Shenzhen Key Laboratory of Energy Electrocatalytic Materials, Guangdong Provincial Key Laboratory of New Energy Materials Service Safety, College of Materials Science and Engineering, Shenzhen University, 1066 Xueyuan Avenue, Nanshan District, Shenzhen 518060, Guangdong, China. E-mail: jll@szu.edu.cn; jwliu@szu.edu.cn

How to cite this article: Liao Y, Xi X, Chen H, Liu J, Fu XZ, Luo JL. The emerging Sr_2FeMoO_6-based electrocatalysts for solid oxide electrochemical cell: synthesis, modulation and applications. *Chem Synth* 2024;4:18. https://dx.doi.org/10.20517/cs.2023.47

Received: 18 Sep 2023 **First Decision:** 2 Jan 2024 **Revised:** 27 Jan 2024 **Accepted:** 20 Feb 2024 **Published:** 5 Mar 2024

Academic Editors: Bao-Lian Su, Xiang-Dong Yao **Copy Editor:** Dong-Li Li **Production Editor:** Dong-Li Li

Abstract

Solid oxide cells (SOCs) are regarded as a promising energy technology due to their large current density, diverse range of fuels, and high energy conversion efficiency. The double perovskite Sr_2FeMoO_6 (SFM) has attracted considerable attention for SOCs due to its tunable structure with superior performance of high conductivity, excellent thermal stability, and remarkable carbon deposition resistance in a reducing atmosphere. However, the electrocatalytic activity of SFM is considerably lower than that of commercial Ni-based SOC electrodes. A timely summary of the synthesis, modulation, and application of SFM perovskites is of great significance for its further development for SOCs. In this review, the methods employed in the preparation of SFM electrocatalysts are introduced first. Then, the advancements in the application of different SFM-based electrocatalysts in the field of SOCs are reviewed, and the research progress in the *in-situ* exsolution of SFM-based electrocatalysts through ion regulation is assessed. Finally, the future issues associated with SFM-based electrocatalysts are addressed in the realm of electrocatalysis, to advance their application.

Keywords: Solid oxide cells, perovskite oxides, Sr_2FeMoO_6, electrocatalysts, element doping, *in-situ* exsolution

INTRODUCTION

The exponential increase in the world's population and the concurrent process of industrialization, coupled with advancements in science and technology, have resulted in a significant surge in the demand for diverse energy sources[1]. The pursuit of clean, secure, and sustainable energy necessitates the advancement of energy conversion devices that exhibit superior efficiency in power generation, the distinct advantage offered by these advanced energy conversion devices when compared to conventional power generation models[2]. Solid oxide cells (SOCs), i.e., solid oxide fuel cells (SOFCs) and solid oxide electrolysis cells (SOECs), can facilitate the mutual conversion of chemical and electrical energy and have a high current density and energy efficiency at a certain temperature, which are ideal energy conversion devices[3,4]. The SOC has an all-solid-state structure consisting of three layers of different types of solid oxide/metal-oxide materials: electrolyte, fuel electrode and air electrode. The electrolyte fraction is usually stacked of micron-level dense oxide particles with high ionic and negligible electronic conductivity. The presence of the electrolyte can avoid the direct contact between the fuel gas and the oxidizing gas and prevent the direct contact between the fuel electrode and the air electrode from an internal short circuit phenomenon. The electrode part (fuel electrode and air electrode) is the site of gas adsorption, diffusion, activation, transformation and dissociation, which is the place where electrochemical reactions occur[5,6]. SOFC can efficiently and cleanly use hydrogen energy and hydrocarbon fuels at high temperatures, convert chemical energy into electrical energy, and complete high-efficiency power generation. Using waste heat and electricity, SOEC can produce hydrogen from water electrolysis on a large scale and electrolysis of CO_2 to high value-added chemicals and fuels, completing the conversion of electricity to chemical energy. The forward operation of the SOFC can generate electricity, and the reverse operation is in the form of SOEC, which means the conversion between SOEC and SOFC can be completed by changing the voltage on the fuel electrode of the SOC[5,7].

One notable advantage of SOC technology lies in its versatility in utilizing a diverse range of fuels, encompassing hydrogen, hydrocarbons, syngas, natural gas, and various other fuel gases[8,9]. The fuel side electrode of SOCs must possess a specific level of catalytic activity towards the fuel gas while also exhibiting a desired level of electrical and ionic conductivity[8,10]. At present, the predominant materials used for SOC electrodes are ceramic-metal composites, specifically the widely used Ni-YSZ (Ni composite yttria-stabilized zirconia) cermet material, as well as mixed ion electronic conductors incorporating perovskites and related structures[11,12]. The conventional Ni-YSZ material exhibits remarkable electrochemical performance and catalytic activity as a SOC fuel electrode[13]. However, because of its susceptibility to splitting C–C and C–H bonds, along with the potential reactivity between Ni and S, carbon deposition and sulfur poisoning may occur on the surface of the fuel electrode[14,15]. Whether in the carbon dioxide reduction reaction (CO_2RR) or the hydrocarbon fuel utilization process, the occurrence of carbon deposition and sulfur poisoning are challenges to the structural stability and activity of the Ni-based electrode[16,17]. Hence, the development of electrocatalysts resistant to carbon deposition and sulfur poisoning is a research hotspot in the field of SOC. Oxide materials with perovskite structures have piqued the interest of many researchers due to their wonderful controllability and anti-carbon deposition ability[9,15,18]. The double perovskite (DP) Sr_2FeMoO_6 (SFM) electrocatalyst has piqued the interest of researchers because of its good electrical conductivity and strong catalytic activity in hydrogen and hydrocarbon fuels[19-21]. However, SFM electrocatalysts cannot exist stably in an oxidizing atmosphere and their electrochemical performance as electrodes is lower than that of Ni-based electrodes[19,22]. Hence, it is imperative to enhance the design of SFM electrocatalysts to enhance their electrochemical performance and redox stability when utilized as SOC electrodes.

SFM electrocatalysts can be prepared via the sol-gel method, the citrate self-combustion method, the solid-state reaction method, the chemical coprecipitation method, the hydrothermal method, and the metal-

organic salt thermal breakdown in the organic solvent. Thin film SFM catalyst can be prepared using the chemical spray thermal deposition and the laser pulse deposition methods[20,21,23-27]. Traditionally, SFM electrocatalysts have been generated by solid-state reactions, but the shape and grain size of SFM electrocatalysts prepared in this manner are difficult to control[28,29]. SFM electrocatalysts utilized in SOC are currently generated via the sol-gel method[19,30-32]. The physical and chemical properties of the SFM catalyst are influenced by different preparation techniques and conditions, which further affect the catalytic activity of the SFM catalyst[33]. As a result, one of the issues that need to be addressed is how to select the preparation method and design the synthesis conditions in various preparation strategies to regulate the physical and chemical properties of SFM-based electrocatalysts.

Surface modification, element doping, and *in-situ* exsolution are important methods to modulate SFM-based electrocatalysts, and their activity and stability can be effectively controlled through these approaches[34,35]. Catalytic activity of SFM electrode can be enhanced by infiltration/impregnation. A liquid phase containing specific components can infiltrate the electrode, and a specific microstructure can be generated on the electrode surface through heat treatment. A suitable nanostructure interface of SFM can enhance the catalytic activity of SFM catalysts more effectively[13,36]. Because of the high valence state of Mo and the structural tolerance of SFM, the doping of ions can cause valence differences between distinct B-site ions, alter the order within the perovskite lattice, and exhibit high catalytic activity, strong redox stability, and quick oxygen transport ability[37,38]. The modulation of the A-site ions in the SFM catalyst can prevent the segregation and enrichment of Sr^{2+} ions on the catalyst surface, stopping the formation of harmful carbonates and preventing the B-site ions responsible for catalytic activity and electron transfer from being blocked[39,40]. In comparison to surface modification, the introduction of B-site ions enables the SFM-based electrocatalyst to anchor alloy nanoparticles (NPs) on the surface of SFM-based SOC electrodes at a lower cost, in a shorter time, and more evenly[37,38]. In short, element doping and surface modification can effectively modulate the electrocatalytic performance of SFM-based electrocatalysts, but exploring how to better regulate the various physical and chemical properties of SFM catalysts by designing the composition of elements and surface modification to aid electrocatalysis is still needed.

To deepen understanding of the electrocatalytic mechanisms and facilitate wider application of SFM in the field of SOCs, a timely review of the synthesis, regulation, and most recent progress of SFM catalysts is of great significance. Herein, this review highlights the most recent advancements in the synthesis, modulation, and applications of SFM-based electrocatalysts in the field of SOCs [Figure 1]. Following an overview of several SFM catalyst synthesis methods, there is a summary of SFM catalyst uses in the field of SOCs and examines how to modulate its catalytic activity through element doping and other means. Afterwards, the origin of the reaction activity of SFM-based electrocatalysts is explored. Finally, the current challenges and possible applications of SFM-based electrocatalysts are proposed to advance their application.

STRUCTURAL CHARACTERISTICS AND SYNTHESIS METHOD OF SR_2FEMOO_6

Structural characteristics of Sr_2FeMoO_6

Crystal structure characteristics of Sr_2FeMoO_6

SFM is a perovskite oxide. As shown in Figure 2A, the ideal SFM has a DP structure and belongs to the cubic Fm-3m lattice[33]. FeO_6 and MoO_6 octahedra are alternately positioned along the three axes of a/b/c to form a lattice skeleton in the face center cubic daughter lattice, the oxygen in the middle bridges is connected with alternating Fe and Mo ions, and the Sr^{2+} ions of large radius occupy the gap between FeO_6 and MoO_6 octahedra[33,41]. At 400 K, due to the large radius of Sr^{2+} ions, FeO_6 and MoO_6 octahedra tended to lower energy structures, and the two transition metal octahedra will be synergistic tilt distortion; the ideal

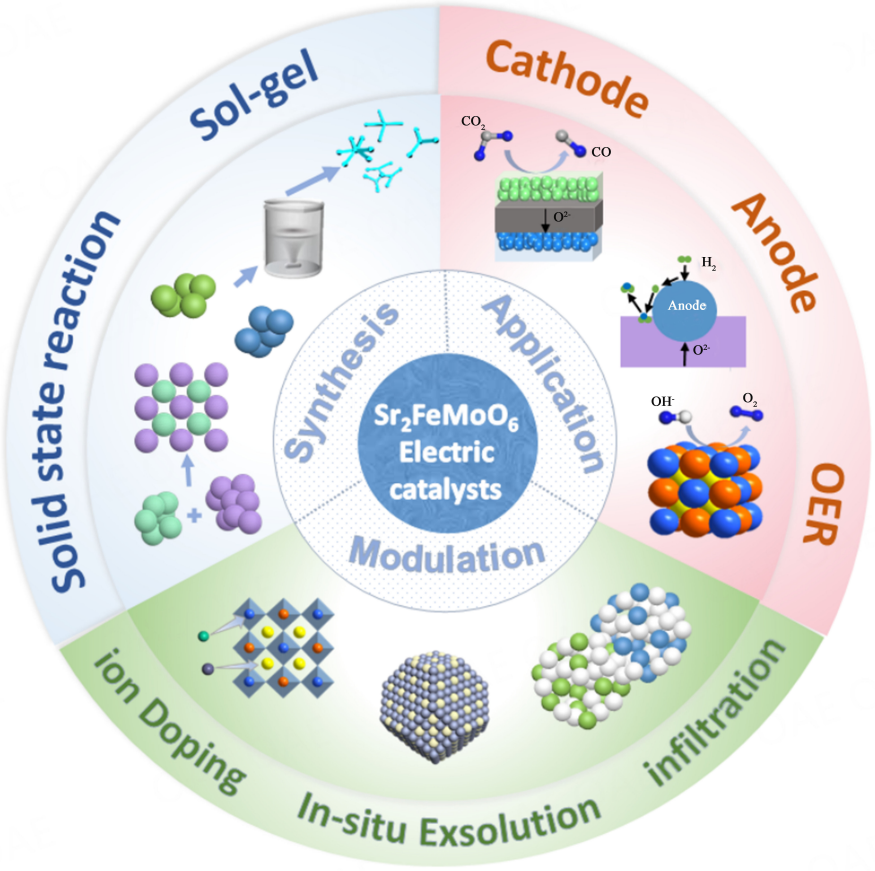

Figure 1. Schematic diagram summary of the application, synthesis methods, and modulation of SFM electrocatalysts. OER: Oxygen evolution reaction; SFM: Sr_2FeMoO_6.

cubic unit cell of SFM thus becomes a tetragonal unit cell I4/m[33]. The lattice parameters of SFM were characterized by a = b = 5.575 Å and c = 7.907 Å. At temperatures over 400 K in a reducing atmosphere, SFM transformed a cubic structure with great symmetry[42]. In this structure, the unit cell parameters were a = b = c = 7.924 Å, which also showed that under the operating temperature of the SOC fuel electrode and the corresponding atmosphere, the SFM exhibited a highly symmetrical cubic structure more conducive to catalysis[42,43]. The structure showed a significant overlap between the transition metal ions Fe and Mo and the oxygen ions, hence promoting efficient electron conduction[44,45]. Additionally, the bond angle between the B–O–B atoms was precisely 180°, further enhancing the conduction of electrons[44,46].

As depicted in Figure 2B, every preparation method enables effective regulation of the concentration of total Fe and Mo atoms in the SFM catalyst. However, the arrangement of Fe and Mo ions within the SFM lattice does not exhibit complete order and alternation. Instead, the presence of anti-site defects (ADs) has been observed, wherein Fe and Mo ions exchange positions; in addition to the conventional Fe–O–Mo bonds, the SFM lattice also contained Fe–O–Fe and Mo–O–Mo bonds[32,47,48]. Furthermore, the presence of ADs, i.e., Fe and Mo, are dislocated from each other, was observed[32]. The existence of ADs can be observed by a series of characterization methods such as high-resolution transmission electron microscopy (HRTEM) and Mössbauer spectroscopy. Affected by the ADs, the electronic structure and semi-metallic properties of SFM were changed. The formation of oxygen vacancies and the number of delocalized electrons in SFM were affected. The magnetic moment size of the ions around the ADs of SFM was changed[32,41,49].

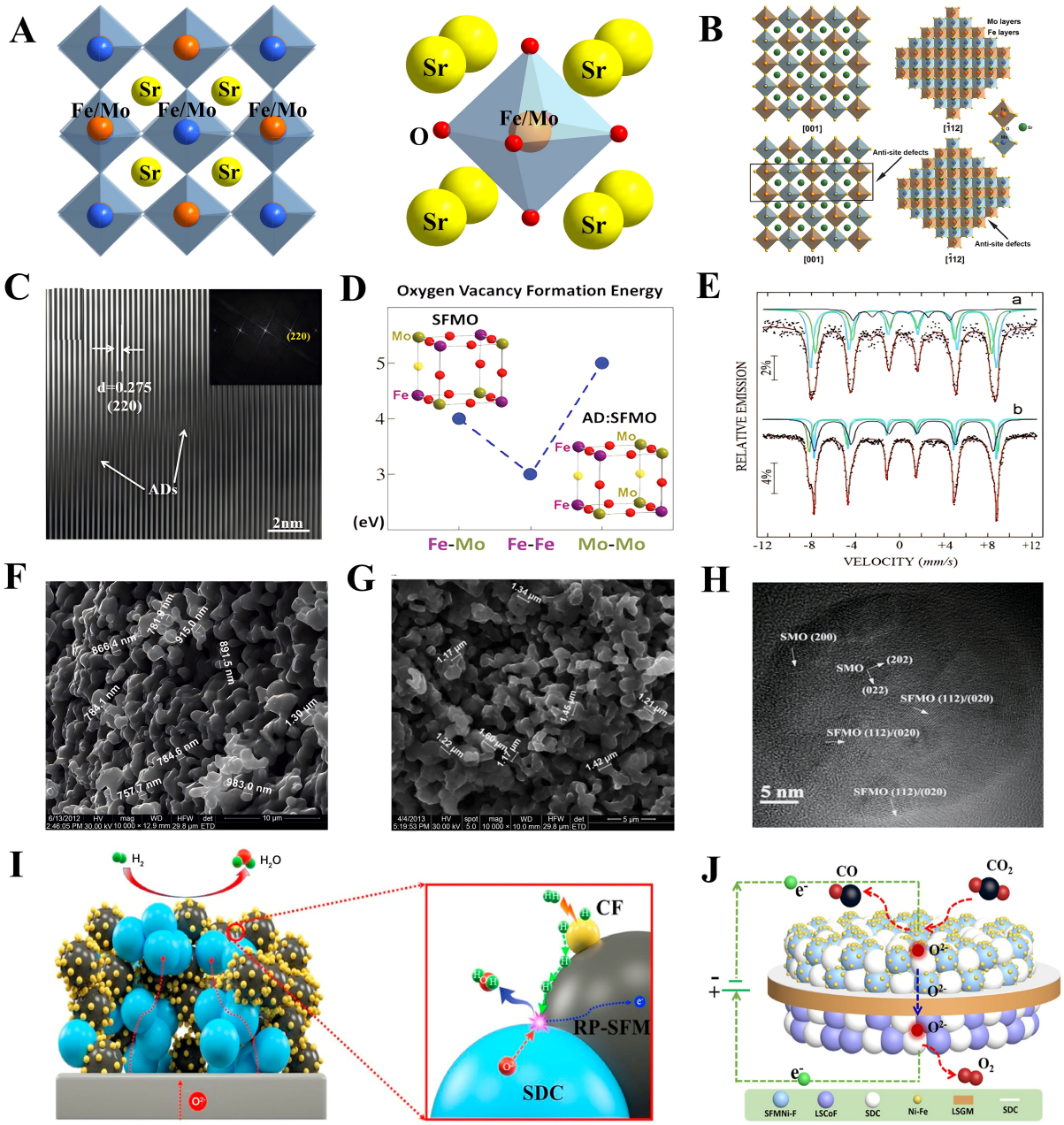

Figure 2. (A) Schematic crystal structure of SFM (plotted by the authors); (B) Schematic diagram of the crystal structure of ideal double perovskite SFM and crystal structure after introducing ADs. Reproduced with permission[32], Copyright 2018, Wiley-VCH; (C) HRTEM image of (220) lattice fringes and corresponding fast Fourier transform. Reproduced with permission[49], Copyright 2021, Wiley-VCH; (D) Oxygen vacancy formation energy for different B–O–B′ bonds in SFM. Reproduced with permission[41], Copyright 2011, Royal Society of Chemistry; (E) Mössbauer spectra of SFM prepared by (a) sol-gel method and (b) solid-state reaction method; (F) Scanning electron microscope diagram of SFM powder prepared by sol-gel method; (G) SEM diagram of SFM powder prepared by solid-state reaction method; (H) HRTEM diagram of SFM prepared by sol-gel method. Reproduced with permission[20], Copyright 2014, Elsevier; (I) Schematic diagram of the reaction of SFM@CF-SDC solid oxide fuel cell anode under hydrogen. Reproduced with permission[67], Copyright 2020, Elsevier; (J) Schematic diagram of solid oxide electrolysis cell cathode electrolysis under CO_2 atmosphere. Reproduced with permission[96], Copyright 2022, American Chemical Society. SFMO: Sr_2FeMoO_6; CF: Co-Fe nanoparticles; RP-SFM: Ruddlesden-Popper phase Sr_3FeMoO_7; SDC: Sm doped ceria; LSGM: $La_{0.2}Sr_{0.8}Ga_{0.8}Mg_{0.2}O_3$; SFM: Sr_2FeMoO_6; ADs: anti-site defects; SEM: scanning electron microscope.

Electron structure characteristics of Sr_2FeMoO_6

At room temperature, SFM attracts attention because of its intrinsic tunneling magnetoresistance, and its electronic structure is impressive. Density functional theory (DFT) is a powerful method for studying multi-electron systems, so it is applied to investigate the electronic structure of SFM. Kimura *et al.* used DFT to calculate the total density of states for SFM with an ordered Fe/Mo arrangement, along with the local density of states of elements. Analysis of the DFT calculation results showed that SFM was semi-metallic at room temperature, and this semi-metallic property rose to 100% spin-polarized charge carriers in the ground state[50].

Furthermore, the electronic structure of SFM was calculated using the spin-polarized GGA + U method, and the effects of the ADs in the synthesis of SFM and the non-stoichiometric ratio of oxygen on the structure and magnetic properties of SFM were studied. The DFT results showed that the saturation magnetization was affected by the proportion of ADs in the stoichiometric SFM and the more ADs, the lower the saturation magnetization, and the spin polarization can be close to 100% when fewer Ads existed. The presence of oxygen vacancies in the SFM reduced the saturation magnetization but retained the semi-metallic properties, meaning that 100% of the spin polarization was retained[42,43]. Based on specific SOC application scenarios, Muñoz-García *et al.* studied SFM materials by DFT + U calculations. ADs can be observed by HRTEM, and the corresponding DFT calculations for SFM also showed the formation energy of oxygen vacancies varies across distinct B–O–B' bonds. Specifically, the total formation energy may be assigned to the following order: $O_v^{Mo\text{-}O\text{-}Mo} > O_v^{Fe\text{-}O\text{-}Mo} > O_v^{Fe\text{-}O\text{-}Fe}$ [Figure 2C and D][41,49]. Due to the low oxygen vacancy formation energy caused by the presence of the ADs. The high concentration of oxygen vacancies in the expected SFM promoted the diffusion of oxygen ions while enhancing the electronic conductivity, which is important for SOC applications[41]. The DFT calculations for SFM show that the nature of various defects in SFM has a profound impact on its application in the magnetic and electrical fields. Therefore, there is no doubt about the importance of SFM synthesis. Regulating the intrinsic structure and properties of SFM by modulating synthesis methods and conditions may be an important direction for modifying SFM in the future.

Chemical synthesis methods of Sr_2FeMoO_6

The synthesis of SFM-based electrocatalysts used in the field of SOC is critical, and different preparation methods affect their structure and properties. There are a lot of methods, among which the solid-state reaction and sol-gel techniques are the main approaches for the synthesis of SFM.

The solid-state reaction method

The solid-state reaction method is a straightforward, widely used, low-cost synthesis approach for inorganic solid materials. Its advantage in synthesizing perovskites lies in its flexibility to produce multi-element phases under high temperature and solvent-free conditions, with strong scalability and simplicity. However, its disadvantage is that the large grain size prepared it yields, which may adversely affect a series of catalytic reactions. The solid-state reaction method for the preparation of DP oxide is typically as follows: after a high-purity stoichiometric oxide of the corresponding element was uniformly mixed and calcined at a specific temperature for a specific time, the precursor of the corresponding substance or the substance itself can be obtained, and then annealed under specific conditions to obtain an oxide with a perovskite structure[29,51]. Traditionally, SFM has been prepared by solid-state reactions. It is widely assumed that the ordered arrangement of Fe and Mo affects the activity of SFM-based electrocatalysts, and different methods determined the degree of order of Fe and Mo[20,21,24,33].

The region in the phase diagram of $SrO\text{-}Fe_3O_4\text{-}MoO_3$ at 1,200 °C 1% H_2/Ar was systematically studied. According to the oxidation metrological ratio and lattice parameter measurement, the solution limit of Mo

in $SrFeO_3$ in air was 17%. The corresponding chemical formula was $Sr_2Fe_{1.34}Mo_{0.68}O_y$, which indicated that SFM cannot exist stably in the oxidizing atmosphere[22]. DP SFM precursor powder composed of two phases ($SrMoO_4$ and SFM) was obtained by calcining SrO, Fe_2O_3, and MoO_3 at 900 °C for 3 h by a solid-state reaction method. Then, the precursor powder was calcined at 1,100 °C by spark plasma sintering, followed by annealing at 5% H_2/Ar reducing atmosphere at 1,200 °C for 2 h to obtain a high-purity SFM phase. Compared with the SFM prepared by the solid-state reaction method, the SFM phase prepared by the sol-gel method had a smaller grain size and showed smaller saturation magnetization strength[21,52,53]. A nanoscale DP SFM was successfully synthesized in air utilizing SrO, Fe_2O_3, and MoO_2 as raw materials, rather than the usual solid-state reaction method. The phase composition and physicochemical properties of the SFM catalyst were significantly affected by the change in the H_2 ratio under a reducing atmosphere[54]. At present, SFM electrocatalysts can be synthesized under unrestricted conditions by solid-state reaction. By manipulating the solid-state reaction conditions, the fast and convenient preparation of high-purity and fine SFM powders may be the basis for future industrial-scale applications.

Sol-gel method

The sol-gel method originated from the phenomenon of combustion of solutions. The size of the various ions and ligands in the solution is usually between 0.1-1 nm, smaller than the size of the solid powder particles. In addition, the spontaneous combustion of the solution involves the generation of a large number of gaseous products, resulting in a more porous and fine structure of the final powder sample than the powder sample prepared by the solid-state reaction method. The porous and fine powder is suitable for SOC, which represents an increase in the density of the reaction site. Therefore, the sol-gel method is widely used in the synthesis of SOC electrode materials[52,53]. This method can be used to create high-purity nanomaterial powder at comparatively low temperatures for SOC electrodes[53,55], and its complete process involved sol preparation, gel gelation of the sol, and solvent removal[53]. When compared to the solid-state reaction method, the sol-gel method had the benefit of being able to control the crystal shape and crystalline size of nano powder, which was highly useful for catalytic reactions[53,55]. Citric acid was used as a coupling in the citrate self-combustion method based on the sol-gel method, and the corresponding metal salt ions were hydrolyzed to form metal citrate. The gelation process was carried out with metal-citrate bonding, resulting in a high uniformity and purity powder[28,52,53].

The microstructure of SFM powder generated by the sol-gel and solid-state reaction methods was examined [Figure 2E-H][20,21]. The average particle size of SFM prepared by the sol-gel method was about 0.9 μm, while the particle size of SFM prepared by the solid-state reaction method was about 1.3 μm. The powder prepared by the sol-gel method was finer than the solid-state reaction method. At the same time, both SFM samples contained a certain amount of $SrMoO_4$, but the content of $SrMoO_4$ in the solid-state sample was more than in the sol-gel sample. As shown by the Mössbauer spectrum, after reduction at the same atmosphere and temperature, the sample prepared by the sol-gel method showed higher magnetization [Figure 2E]. The ultrafine field value of the Mössbauer spectrum of the sample that the SFM prepared by the sol-gel method showed that SFM formed an ordered DP structure. The ultrafine field value of the Mössbauer spectrum of the sample proves that the SFM prepared by the solid-state method obtained a slightly disordered structure. The reason was attributed to the exchange positions of Fe and Mo ions. When Fe and Mo ions exchange positions, Mo's $4d^1$ electrons and Fe^{3+} $3d^5$ electrons spin polarizations were reversed, while the electron delocalization of the Mo ions represented a decrease in charge density, resulting in a decrease in the overall spin density[20,21]. The citrate sol method was used to prepare DP SFM powder with a small grain size, and the effect of sol pH on the order of B-site ions in SFM powder was studied. The results showed the purity of SFM powder prepared from precursor sols with pH 7.5 and 9.0 was the highest, and the sample calcined at 1,050 °C was a quadrangular I4/m structure. After calcination at 975 °C, the SFM

sample exhibited a monoclinic structure[30]. By varying the flow rate of the reducing gas (5% H_2/Ar), the synthesis of SFM was studied under various gas flow rates. It was found that SFM prepared at different flow rates exhibited diverse properties under the influence of magnetic fields, which were related to the ADs, crystallinity, and oxygen vacancy of various SFM samples[56]. The grain size, ADs, and oxygen vacancy concentrations of perovskite oxides were controlled by modulating the synthesis conditions of the sol-gel method (e.g., pH, temperature, gas flow rate) to promote its application in electrocatalysis by improving the intrinsic properties and structure of the materials. At the same time, it is worth noting that the magnetization intensities of SFM catalysts prepared by different preparation methods are different[23,54,57]. This may mean that improving the spin of Fe in SFM by specific methods (e.g., atomic doping, lattice strain, and magnetic field coordination) could reduce the chemical reaction energy barrier and promote the occurrence of reactions.

Other synthesis method

In addition to the traditional sol-gel and solid-state reaction methods, there are numerous ways to prepare SFM catalysts. These techniques were typically used to produce SFM with specific characteristics. For instance, the microwave radiation method enhanced the diffusion and nucleation process of ion precursors in the process of a synthetic sol, and the grain size was reduced[28]. The effects of several synthesis methods on the number of oxygen vacancies in SFM catalysts were investigated. It was discovered that the number of oxygen vacancies in SFM catalysts generated by the thermal decomposition of metal salts using organic sols > the number of oxygen vacancies in sol-gel-produced SFM catalysts > the number of oxygen vacancies in SFM catalysts made by the hydrothermal method. The photocatalytic activity of SFM catalysts prepared by the corresponding preparation method also followed the above rules[26]. The X-ray photoelectron spectroscopy results also showed that different preparation conditions and methods had effects on the valence state of transition metal ions and the content of lattice oxygen and interstitial oxygen in SFM. The above research demonstrated that increasing the amount of oxygen vacancies in SFM catalysts is an extraordinary strategy for improving catalytic performance[26].

Collectively, to construct the relationship between synthesis methods, structure, and purity, it is necessary to summarize various preparation methods and consider their influence on SFM electrocatalysts [Table 1]. Although the solid-state reaction method has the significant advantages of being simple, direct, and low-cost, it generates large-size powder grains, which is not conducive to the catalytic reaction to a certain extent. In contrast, the sol-gel method is widely used in the SOC field because of its characteristics and ability to control the size of grains. Different preparation methods affected the physicochemical properties of SFM electrocatalysts, especially the ADs and oxygen vacancy concentrations, which were closely related to the catalytic activity of SFM. The magnetic properties of SFM have also been continuously studied, but whether there is a certain relationship between magnetic properties and electrocatalysis still needs to be investigated. The sol-gel method is more suitable for laboratory-level production, whereas the solid-state reaction method is better suited for industrial-scale production. Therefore, balancing performance and scale of production is undoubtedly one of the difficulties encountered in future SFM applications.

APPLICATION OF SR_2FEMOO_6 IN SOLID OXIDE CELLS

Sr_2FeMoO_6 electrode materials for SOC anodes

SFM electrocatalysts are commonly used in solid oxide electrochemical cells, especially anodes for medium and high-temperature fuel cells. Under reducing conditions, DP SFM was stable and exhibited splendid catalytic activity for fuel oxidation and high conductivity. SFM anodes demonstrate better resistance to sulfur poisoning and carbon deposition than Ni-based fuel electrodes in the use of hydrocarbon fuel[19,65,66]. The principle of the SFM-based anode using hydrogen fuel is that the anode accepts oxygen ions conducted

Table 1. The summary of Sr_2FeMoO_6 (SFM) synthesis methods

Synthetic method	Precursor			Ligand /medium	Reaction conditions			Grain size (nm)	ADs (%)	Oxygen vacancies (O_{occ})	Ref.
	Sr source	Fe source	Mo source		Temperature [°C]	Time [h]	Atmosphere				
Sol-gel method	$(CH_3CO)_2Sr$	$Fe(NO_3)_3·9H_2O$	MoO_2	Citric acid monohydrate	1,100 + 1,200	3 h + 2 h	Air + 5% H_2-Ar	~900	-	-	[20]
	$Sr(NO_3)_2$	$Fe(NO_3)_3·9H_2O$	$(NH_4)_6Mo_7O_{24}·4H_2O$	$C_6H_8O_7·H_2O$	900 + 1,150	10 h + 12 h	Air + 5% H_2-Ar	~800	~10.96%	-	[56]
	$Sr(NO_3)_2$	$Fe(NO3)_3·9H_2O$	$(NH_4)_6Mo_7O_{24}·4H_2O$	Citric acid monohydrate	900	-	5% H_2-Ar	-	-	-	[26]
	$Sr(NO_3)_2$	$Fe(NO_3)_3·9H_2O$	$(NH_4)_6Mo_7O_{24}·4H_2O$	Citric acid /$NH_3·H_2O$/H_2O	450 + 750	1.5 h + 3 h	Air + 5% H_2-Ar	~250	5.1%	-	[23]
	$Sr(NO_3)_2$	$Fe(NO_3)_3·9H_2O$	$(NH_4)_6Mo_7O_{24}·4H_2O$	Citric acid	600 + 800 + 1,200	5 h + 4 h + 12 h	Air + 5% H_2-Ar	-	-	-	[24]
	$Sr(NO_3)_2$	$Fe(NO_3)_3·4H_2O$	Mo powder	Citric acid /$NH_3·H_2O$/H_2O	500 + 1,050	2 h + 38 h	Air + 5% H_2-Ar	~200	~10%	-	[30]
	$Sr(OH)_2·nH_2O$	$Fe(NO_3)_3·9H_2O$	$(NH_4)_6Mo_7O_{24}·4H_2O$	Acetic acid /acetone /oxalic acid	1,000	8 h	N_2	~1,000	-	-	[58]
	$(CH_3CO)_2Sr$	$Fe(NO_3)_3·9H_2O$	MoO_2	Citric acid monohydrate	900 + 1,200	3 h + 2 h	Air + 5% H_2-Ar	~1,100	-	-	[21]
	$Sr(NO_3)_2$	$Fe(NO_3)_3·9H_2O$	$(NH_4)_6Mo_7O_{24}·4H_2O$	Citric acid /$NH_3·H_2O$	700 + 1,000	6 h + 3 h	Air + 3% H_2-Ar	-	-	-	[59]
	$Sr(NO_3)_2$	$Fe(NO_3)_3·9H_2O$	MoO_2	Citric acid	900 + 1,200	3 h + 3 h	Air + 5% H_2-Ar	~340	-	-	[28]
	$Sr(NO_3)_2$	$Fe(NO_3)_3·9H_2O$	$(NH_4)_6Mo_7O_{24}·4H_2O$	Citric acid /$NH_3·H_2O$/H_2O	500 + 700	6 h	Air + 1% H_2-Ar	~100	-	-	[60]
Solid-state reaction method	SrO	Fe_2O_3	MoO_3	-	1,100	2 h	5% H_2-Ar	~200	16.55%	-	[61]
	$SrCO_3$	Fe_2O_3	MoO_3	-	-	-	-	-	-	-	[25]
	$SrCO_3$	Fe_2O_3	MoO_3	Isopropyl-alcohol	1,000 + 1,150	3 h + 3 h	O_2 + 5% H_2-N_2	-	-	-	[62]
	$SrCO_3$	Fe_2O_3	MoO_3	Ethanol	900 + 1,060	4 h + 4 h	Air + 5% H_2-Ar	-	-	-	[47]
	$SrCO_3$	Fe_2O_3	MoO_3	-	900 + 1,200	3 h + 7.5 h	Air + 5% H_2-Ar	-	14%	5.58	[63]
	SrO	Fe_2O_3	MoO_3	Ethanol	900 + 1,200	3 h + 2 h	Air + 5% H_2-Ar	~1,200	-	-	[21]
	$SrCO_3$	Fe_2O_3	MoO_3	-	900 + 1,200	3 h + 1.5 h	Air + 6% H_2-N_2	-	-	-	[64]
	SrO	Fe_2O_3	MoO_3	-	1,100 + 1,200	3 h + 2 h	Air + 5% H_2-Ar	~1,300	-	-	[20]
Hydrothermal preparation method	$Sr(NO_3)_2$	$Fe(NO_3)_3·9H_2O$	$(NH_4)_6Mo_7O_{24}·4H_2O$	Na_3Cit /deionized water	1,150	8 h	5% H_2-Ar	-	-	-	[26]
Thermal decomposition of a metal-organic salt in an organic solvent	$C_{10}H_{14}SrO_4$	$C_{15}H_{21}FeO_6$	$C_{10}H_{14}MoO_6$	Oleic acid, oleyl amine, benzyl ether	900	5 h	5% H_2-N_2	-	-	-	[26]

from the cathode, and hydrogen dissociates into protons at the corresponding active site and combines with conducted oxygen ions to form water molecules [Figure 2I]. The process converts chemical energy into electrical energy, and the fuel oxidation process becomes more complex based on the diversification of fuel gases[67].

The process of direct methane and hydrogen utilization when SFM materials were used as SOFC anodes was investigated. It was discovered that SFM as an anode exhibited power densities of 864.7 and 604.8 $mW·cm^{-2}$ under a hydrogen atmosphere and a dry methane atmosphere at 850 °C, demonstrating the excellent catalytic activity of SFM for hydrogen and methane[19]. The properties of SFM breakdown into $SrMoO_4$ and $SrFeO_3$ in a high-temperature oxidation environment were investigated, and the redox stability of the material was derived from the maximum solubility of SFM in the air, which can only exist in the air at most $Sr_2Fe_{1.34}Mo_{0.68}O_6$ single phase[22]. $Sr_2Fe_{1.5}Mo_{0.5}O_6$ (SF1.5M) can exist stably in the air or a reducing atmosphere when applied to symmetric SOFCs[49,68]. The polarization resistance of SF1.5M in a humidified hydrogen atmosphere was 0.21 $Ω·cm^2$ at 850 °C, 0.27 $Ω·cm^2$ at 800 °C, and 0.46 $Ω·cm^2$ at 750 °C. The excellent redox stability and good properties of SF1.5M make it a promising electrode material in SOC electrodes[22,68-70]. Although SFM as a SOFC anode shows acceptable hydrogen oxidation and methane splitting capabilities, its activity is still lower than that of Ni-YSZ anodes. Therefore, the current research still focuses on how to improve the catalytic activity of SFM-based electrodes.

Sr_2FeMoO_6 electrode materials for SOC cathodes

DP SFM can be used as the cathode of SOEC. CO_2 fuel gas is employed by SFM-based SOEC cathodes [Figure 2J][7,9,71]. CO_2 takes electrons in the cathode to form CO and oxygen ions, while oxygen ions are transported to the anode via the electrolyte. The oxygen ions are sent to the anode and lose electrons to produce oxygen molecules[7,9].

SFM is developed as a SOEC cathode with a current density of roughly 0.8 $A·cm^{-2}$ at 800 °C and a potential of 1.5 V under pure CO_2[31]. SFM and $La_{0.2}Sr_{0.8}Ga_{0.8}Mg_{0.2}O_3$ (LSGM) were combined as electrodes for symmetrical cells, showing high current density and good stability. 20% SFM-LSGM|LSGM|20% SFM-LSGM were prepared for CO_2 electrolysis by simple casting strip and permeation methods. At 800 °C, the current density was 1.24 $A·cm^{-2}$ at an applied potential of 1.5 V. Under a pure CO_2 atmosphere, the cell ran for 53 h without carbon deposition[18]. Furthermore, based on the instability of SFM in an oxidizing atmosphere, redox-stable SF1.5M was proposed for SOEC electrodes. The use of SF1.5M for hydrogen production by water electrolysis on the fuel electrode of SOEC was studied. At 900 °C, with absolute humidity of 60%, and applied voltage of 1.3 V, the electrolysis current was 0.88 $A·cm^{-2}$ and the hydrogen production rate was 380 $mL·cm^{-2}·h$, while also demonstrating outstanding stability due to the stability of SF1.5M itself in a high-temperature redox atmosphere[69]. Compared to SFM, SF1.5M not only had good redox stability but also exhibited faster reaction kinetics. When running at 800 °C, the SF1.5M reversible SOC had a high power density of 1.24 $W·cm^{-2}$ under hydrogen and a significant electrolytic current of 1.5 $A·cm^{-2}$ at 1.5 V when utilizing CO_2 as fuel[49]. The reason for the fast kinetics of electrocatalytic reaction of SF1.5M was that increasing the Fe content in SF1.5M enhanced the metal-oxygen hybrid state, which promoted the p-band center of lattice oxygen towards the Fermi level and boosted the intrinsic catalytic activity of SF1.5M[49].

Not only for SOEC cathodes, SFM can also be applied to SOFC cathodes. SFM also exhibited certain oxygen reduction activity when used as a SOFC cathode. SFM|LSGM|SFM was prepared with a symmetrical configuration, and it was found that the cell exhibited power densities of 0.025, 0.125, and 0.25 $W·cm^{-2}$ at 700, 750 and 800 °C under pure hydrogen atmosphere. Although SFM exhibits good activity in CO_2RR, it is

still too early to be truly applied. Manipulating SFM to achieve better activity and stability is the future development direction.

Sr_2FeMoO_6-based catalyst for oxygen evolution reaction

Perovskite oxides have already emerged as promising oxygen evolution reaction (OER) catalysts due to their great structural controllability and mixed conductivity[72-75].

Previous studies showed that doping can significantly enhance the performance of OER. The presence of oxygen vacancies enhanced the OER performance of perovskite catalysts. For instance, the SFM-based triple perovskite oxide $Sr_3NiFeMoO_9$ required 260 mV to reach an anode current density of 10 $mA{\cdot}cm^{-2}$ under alkaline conditions, which was much lower than SFM's overpotential of 297 mV. And the triple perovskite $Sr_3NiFeMoO_9$ showed the smallest Tafel slope (42.3 $mV{\cdot}dec^{-1}$) compared to SFM (64.5 $mV{\cdot}dec^{-1}$)[76]. In addition, *in-situ* exsolution plays an important role in the OER performance enhancement. SFM-based $Sr_2Fe_{1.3}Ni_{0.2}Mo_{0.5}O_6$ (SFNM) can produce oxygen vacancies and *in-situ* exsolution of Fe-Ni NPs due to treatment under a reducing atmosphere, reaching a current density of 10 $mA{\cdot}cm^{-2}$ at an overpotential of 360 mV, and a Tafel slope of 59 $mV{\cdot}dec^{-1}$, showing excellent OER activity[77]. The perovskite oxide $Sr_{1.92}Fe_{0.92}Co_{0.08}MoO_6$ based on SFM showed that Co can be segregated on the surface of SFM lattice to generate Co NPs and an amorphous phosphating layer can be obtained by phosphating[78]. The generated Co/SFM-P had outstanding activity and stability for OER, which came from the strong synergy between Co NPs and the oxide substrate[78]. Because of its unique properties, SFM was expected to become a material capable of replacing noble metals-based catalysts. However, their activity is still not as good as that of traditional noble metal-based OER catalysts[79,80]. The OER activity of SFM-based catalysts still needs further improvement.

Generally, the applications of SFM catalysts in the field of electrocatalysis have great potential. However, compared to Ni-based electrodes, they still face some challenges due to insufficient activity. To improve the catalytic activity of the SFM catalyst and promote its application in SOC, it is necessary to control its crystal and electronic structure, deepen the understanding of the catalytic mechanism, and optimize its surface and interface design.

Modulation of SOC Sr_2FeMoO_6-based catalysts

Currently, there are three main methods to improve the electrochemical performance of SFM-based catalysts for SOC electrode materials, namely surface modification, element doping, and *in-situ* exsolution, among which element doping and *in-situ* exsolution strategies based on element doping are current research hotspots.

Surface modification

SFM-based catalysts must have good chemical stability, thermal stability, and mixed conductivity at SOC working temperatures and in various atmospheres. As a result, one important approach to improve the performance of SFM-based electrocatalysts is surface modification (impregnation/infiltration). Impregnation/infiltration refers to the use of a liquid phase containing the desired components to infiltrate the porous SOC electrode substrate and then carry out a certain heat treatment to produce a specific nanostructured interface on the electrode surface so that the impregnated electrode exhibits lower resistance and better electrochemical performance[13,36,81]. SFM was impregnated with Pd or Co-Ni-Mo on the surface using the glycine-mediated impregnation method and used for SOFC electrodes. The Pd and Co-Ni-Mo-impregnated SFM had R_p values of 0.087 and 0.060 $\Omega{\cdot}cm^2$ under humidified H_2 at 800 °C, respectively, while the produced single cells had power densities of 1,066 and 480 $mW{\cdot}cm^{-2}$ in hydrogen and methane atmospheres at 800 °C, respectively. The results showed that the impregnation effectively improved the catalytic activity of the SFM electrode[82].

At present, there are not many studies on the surface modification of SFM. The surface modification studies of SF1.5M are more diverse. Wang *et al.* increased the CO_2RR activity of SF1.5M by impregnating nano-sized Pr_6O_{11} on the surface of the SF1.5M electrode[83]. Zhang *et al.* successfully improved the electrochemical performance of SOEC by constructing a composite heterogeneous interface between alkaline earth metal oxide and SF1.5M electrode through infiltration[84]. It is not difficult to see that the current researches are mainly focused on the impregnation of oxides (e.g., Gd-doped ceria, alkaline-earth metal oxide, and Pr_6O_{11}) or metals (e.g., Ni and Ru) on the surface of the electrode to form an oxide-oxide/metal-oxide heterojunction[85-87]. Hence, in terms of surface modification, promising catalysts are SFM electrodes covered with oxide/active transition metal particles. However, many scientific questions still exist in surface modification, such as how surface modification interacts with the SFM catalyst matrix to affect electrode reactions and how nano coatings composed of surface modification affect the electrocatalytic process.

Element doping

In the regulation of SFM-based catalysts, element doping is a research hotspot. Firstly, based on the structural characteristics of perovskite, element doping can well regulate the structure of SFM, thereby improving its intrinsic activity. Secondly, the *in-situ* exsolution strategy based on element doping can construct the metal-oxide heterogeneous interface from the bottom up, which improves the performance of the SOC electrode while maintaining long-term stability[8,45,88]. The basic principle of elemental doping is doping various elements based on the different actions of A, B, and O ions in the perovskite oxide structure. The partial replacement of their ions has the effect of regulating the chemical composition of perovskite and the lattice structure, allowing the structure's oxygen vacancy concentration to be adjusted, the crystal geometry to be improved, and the performance of electron conduction to be promoted[10,89].

Element doping at various locations can result in a variety of outcomes. The A-site ions are primarily responsible for the stability of the perovskite structure. Doping and defects of A-site ions can also affect the oxygen conductivity of the material itself by affecting the generation of oxygen vacancies. Because A-site doping alters the ratios of Fe^{2+}/Fe^{3+} and Mo^{5+}/Mo^{6+} in SFM, it can affect the crystal structure and electronic characteristics of perovskite, and hence its chemical properties[90,91]. Doping of B-site ions is the most common doping strategy; using different types and amounts of transition metal ions in the B-site of perovskite, the conduction of electrons can be adjusted. The *in-situ* exsolution strategies differ from conventional element doping methods. They introduce active transition metals into the interior of the crystal lattice to cause phase transformation of the main phase perovskite under specific conditions, hence optimizing the surface and interface structure of the perovskite[37,92-96].

A-site modulation

Substitution of A-site ions, whether partial or complete, is an effective approach for regulating the electrocatalytic performance of SFM-based electrocatalysts. The A-site ion Sr^{2+} in SFM can be partially or entirely substituted by alkaline metals (e.g., Na and Cs) or lanthanides (e.g., Ce and La) to achieve increased activity. Since the ionic radius of Sr, Ba, and Ca are similar, the A_2FeMoO_6 (A = Ca, Sr, Ba) were investigated as a potential anode material for SOFCs, and the performance of the anode materials followed Ca_2FeMoO_6 < Ba_2FeMoO_6 < SFM[65]. At 850 °C, the maximum power density of SFM anode cells was 831 mW·cm^{-2} in dry H_2 and 735 mW·cm^{-2} in commercial city gas, respectively[65]. The high conductivity of A_2FeMoO_6 (AFM, A = Ca, Sr, Ba) as the SOFC anode was studied, and they have good structural stability under a high-temperature reducing atmosphere, with no phase decomposition, and demonstrate good thermal matching

with the electrolyte material. The Ba_2FeMoO_6 and SFM anodes were evaluated from the performance point of view, and the maximum power densities under a hydrogen atmosphere were 605 and 757 $mW·cm^{-2}$, respectively[66]. The aforementioned results suggest that a complete substitution of the A-site ion strategy may be a good element doping strategy.

The partial doping strategy of A-site ions of SFM is more mainstream. The effects of potassium doping SFM on crystal structure and magnetism were investigated. It was discovered that potassium doping effectively regulated the ADs in $Sr_{2-x}K_xFeMoO_6$ ($0 \leq x \leq 0.04$). The presence of ADs affected the formation energy of oxygen vacancies, and the large radius of potassium ions caused changes in the crystal structure, making the crystals more symmetrical and favorable for magnetic[41,97]. DFT calculation was used to study the crystal and electronic structure of La^{3+} doped with SFM and the electrochemical performance of the $Sr_{2-x}La_xFeMoO_6$ anode. With the doping of La, $Sr_{2-x}La_xFeMoO_6$ gradually changed from the tetragonal crystal system to the orthogonal crystal system with higher symmetry. The introduction of La ions served to increase the additional electrons on the e_g and t_{2g} anti-bond orbitals of Fe/Mo ions. The increase of electrons in the antibonding orbital led to the increase of oxygen vacancy concentration of $Sr_{2-x}La_xFeMoO_6$, so $Sr_{2-x}La_xFeMoO_6$ had excellent performance when used as an anode of SOFC[98,99]. La doping influenced not only the electrical structure but also the crystal structure of SFM. The effects of La on crystal structure, grain morphology, and electrical properties of SFM were investigated. The doping of La boosted the number of grain nucleation centers, which, in turn, increased small-sized grains and refined the grains. The resistance of the La-doped SFM was lower than that of the matrix SFM[99]. In summary, partial substitution of A-site ions can effectively regulate the crystal/electronic structure of SFM.

In comparison to the doping strategy, regulating the defect number of A-site ions can promote the valence state change of the B-site ions to form additional oxygen vacancies. Artificially creating A-site defects may be able to drive the *in-situ* exsolution of B-site transition metal ions, significantly improving the activity of SFM-based catalysts[100-102]. $Sr_xFe_{1.5}Mo_{0.5}O_6$ (x = 1.9-2.0) was investigated as a SOFC cathode. It was discovered that as the number of defects increased, the unit cell characteristics became orthogonal. Simultaneously, the rise in A-site defects caused a shift in the proportion of redox couples of $S_xF1.5M$, which directly influenced the material's conductivity. $S_{1.95}F1.5M$ was constructed as a SOFC cathode, with the maximum power density reaching 1,083 $mW·cm^{-2}$ at 800 °C[103]. Under certain conditions, NPs can be exsolved *in-situ* on the surface of perovskite oxides with A-site defects and the doping of transition metal ions[104]. Feng *et al.* studied Ni-doped $Sr_{2-x}Fe_{1.4}Ni_{0.1}O_6$ (x = 0-0.1) with A-site defects and discovered Ni NPs in X-ray diffraction (XRD) and scanning electron microscopy[104]. It can be inferred that *in-situ* exsolution can be promoted by combining the two strategies of regulating A-site defects and B-site doping.

Obviously, the regulation of the A-site ions of SFM is mainly focused on doping and defect modulation. The electronic structure of SFM can be regulated by doping elements with a similar ion radius to Sr (e.g., IA main group elements, IIA main group elements, lanthanides), and then, the electrochemical reaction process of SFM to fuel gas can be promoted. The preferred A-site doping element is La. The doping of La successfully modulated the electronic structure of SFM, reduced the oxygen vacancy formation energy of SFM, and improved its catalytic activity for methane and hydrogen[98]. In addition, the radii of Pr and Sr are similar, and there are related research suggests excellent electrochemical performance of Pr-doped SF1.5M excellent[105,106]. Therefore, Pr is also the preferred choice among the A-site elements. As Pr has f electrons, how the doping of Pr affects the electronic structure of SFM needs to be explored. The unfavorable segregation of Sr can be inhibited by regulating the defects of Sr ions, and the combination of this strategy and B-site ion control can well promote the *in-situ* exsolution of NPs. Therefore, the A-site ion modulation strategy has a wide range of application prospects.

B-site modulation

Modulating the types of B-site ions in perovskite oxides is a widely employed approach in the field of SOC material engineering. There are two primary methods for regulating the B-site ions of SFM-based electrocatalysts. The first approach involves optimizing the Fe/Mo ratio, which has been shown to significantly enhance the electrochemical performance of SFM as a SOC electrode[68,107]. The second method involves doping the SFM material with various transition metal ions, which actively modifies the crystal and electronic structure of SFM catalysts, thereby promoting electrocatalytic activity[37,49,69,108-110]. Additionally, when transition metal-doped SFM electrocatalysts (e.g., Ni, Cu, and Co) are exposed to a reducing atmosphere, *in-situ* exsolution occurs, resulting in the formation of a metal-oxide heterogeneous interface. The strong synergy between the exsolved NPs and oxide substrate changes the interaction between the catalyst and small molecules, promoting the reaction on the surface of the electrode[37,49,69,108-110]. NPs formed through this process become embedded on the surface of the perovskite matrix, and the resulting metal-oxide interface exhibited enhanced stability and electrocatalytic performance[37,108-110].

The maximum solubility of Mo in air was determined by utilizing previously reported oxidation metrology and lattice parameter measurements[22]. Reversible phase transitions of SFM under oxidative and reductive conditions were also demonstrated [Figure 3A]. Despite the formation of a mixed phase (SFM and $SrMoO_4$) in SFM under oxidizing conditions, the associated insulating phase ($SrMoO_4$) disappeared under reducing conditions. It is inferred from Figure 3A that although the phases present in the SFM are different under redox conditions, the performance of the SFM used for SOC may be unchanged after reduction[19]. The cycle number test of SFM in dry CH_4 and H_2 also showed that SFM had good stability in CH_4 and H_2, and the maximum power density of SFM in CH_4 and H_2 decreased slowly within 20 cycles. The test in CH_4 showed that compared to the traditional Ni-based anode, SFM had better stability [Figure 3B][19]. The conductivity test of SFM also showed that the generation of $SrMoO_4$ affected the conductivity of SFM. The conductivity of SFM was low in an air atmosphere, with only 25 $S{\cdot}cm^{-1}$ at 800 °C. And the conductivity of SFM (sintered in H_2/Ar) was high in hydrogen atmosphere, with nearly 250 $S{\cdot}cm^{-1}$ at 800 °C [Figure 3C][82]. Even in hydrogen, the conductivity of SFM synthesized under various conditions was quite different, which also confirms the importance of synthesis methods for SFM[82]. Based on the maximum solubility of Mo in air, the SF1.5M was proposed. It was observed that SF1.5M exhibited high conductivity both in air and a reducing atmosphere and also displayed certain catalytic activity[22,69-71]. Figure 3D presents the XRD pattern of SFM and SF1.5M calcined in air or H_2, with a_1 representing the pattern of SFM obtained from air calcination, a_2 and a_3 representing patterns of SF1.5M obtained from calcination in air and under H_2 atmosphere, respectively. It can be seen that SF1.5M remained stable in phase structure compared with matrix SFM[69-71]. Liu *et al.* used SF1.5M to make a symmetrical cell. By switching the fuel-side electrode gases (hydrogen and air and emptying the fuel cell system with nitrogen), the authors tested the maximum power density of the SF1.5M symmetrical cell and the electrochemical impedance spectrum after each redox cycle. There is no significant change in the electrochemical impedance spectrum and maximum power density of SF1.5M after five redox cycles of up to 40 h, which showed the excellent stability of SF1.5M [Figure 3E][68]. To assess the performance of SF1.5M as SOFC anodes, a cyclic test method was employed [Figure 3F]. By switching the fuel-side electrode gases (hydrogen and CH_4, and emptying the fuel cell system with nitrogen). After 200 h and 16 redox cycles, the maximum power density of the SF1.5M symmetrical cell remained stable[70].

The intrinsic factors of SF1.5M electrochemical performance improvement were studied[49]. The enhancement of metal-oxygen hybridization in SF1.5M led to an increase in the oxidation state of Fe, causing the p-band center of lattice oxygen to shift towards the Fermi energy level. Consequently, the formation of oxygen vacancies and the migration of oxygen ions were promoted by the doping of Fe,

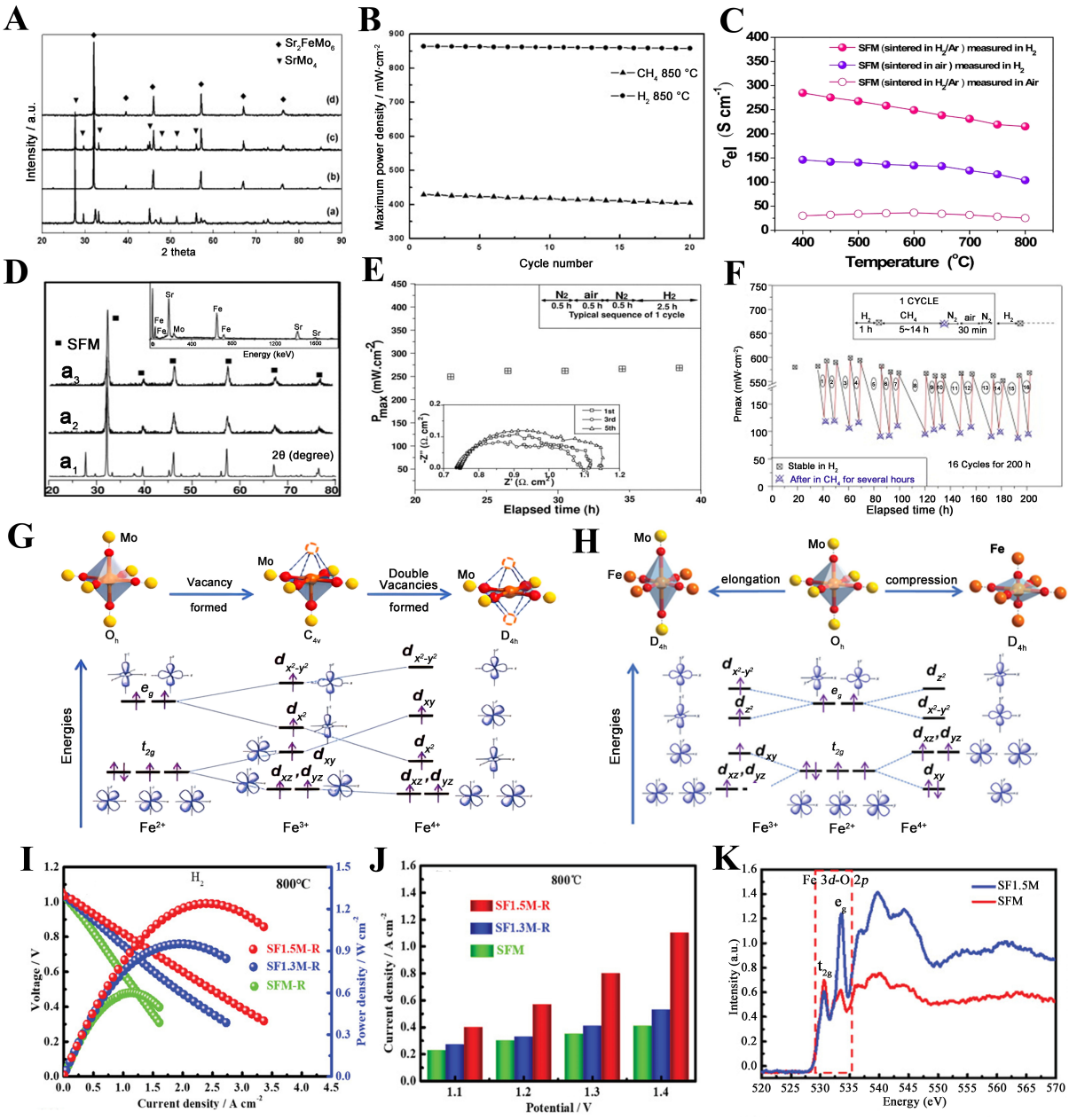

Figure 3. (A) XRD patterns of (a) SFM precursor and (b) SFM-R powder and (c) SFM-R-O (O means oxidize) powder and (d) SFM-R-O-R (R means reduce) powder; (B) Cycle number and power density test of SFM at 850 °C under CH_4 and H_2 atmosphere. Reproduced with permission[19], Copyright 2011, Elsevier; (C) Conductivity changes of SFM synthesized under different conditions (measured in hydrogen and air). Reproduced with permission[82], Copyright 2016, Elsevier; (D) XRD of (a_1) SFM and (a_2) SF1.5M produced following 5 h calcination in air at 1,000 °C; (a_3) SF1.5M as synthesized after 24 h of treatment at 1,000 °C in H_2 (SFM in the figure means SF1.5M in this review). The EDX analysis of SF1.5M powders is shown in the inset; (E) Redox stability test of SF1.5M. Reproduced with permission[68], Copyright 2010, Wiley-VCH; (F) 16 cycles of switching the fuel gas between hydrogen, air, and CH_4, the stability of the SF1.5M|LSGM|SF1.5M single cell at 850 °C. Reproduced with permission[70], Copyright 2011, Elsevier; (G) The occupation of d electrons for Fe in the ideal SF1.5M and SF1.5M with oxygen vacancies; (H) Illustration of SF1.5M's unusual coordinating environment; (I) Electrochemical performance of SFXM (X = 1, 1.3, 1.5) single cells under a hydrogen atmosphere of 800 °C; (J) Electrochemical performance of SFXM (X = 1, 1.3, 1.5) single cells under a CO_2 atmosphere of 800 °C; (K) O K-edge X-ray absorption spectroscopy of SF1.5M and SFM. Reproduced with permission[49], Copyright 2021, Wiley-VCH. XRD: X-ray diffraction; SFM: Sr_2FeMoO_6; EDX: energy dispersive X-ray spectroscopy; SFXM: $Sr_2Fe_xMo_{2-x}O_6$ (x = 1, 1.3, 1.5).

resulting in enhanced catalytic activity of SF1.5M[49,111]. The d electron occupancy of Fe ions in the presence of oxygen-free vacancies in SF1.5M was investigated, utilizing crystal field theory, which examined the impact of Fe ions on structural and energetic changes resulting from the substitution of Mo ions [Figure 3G]. The results showed that the doping of Mo by Fe affected the generation of oxygen vacancies[49]. The investigation of the distinctive coordination environment of SF1.5M was conducted using crystal field theory. The structural modifications observed in SF1.5M were attributed to the augmentation of Fe substitution for Mo, and experimental and simulation analyses confirmed that the Fe^{4+} content in SF1.5M exceeded that of SFM [Figure 3H][49]. SF1.5M electrodes showed a high peak power density of 1.24 $W{\cdot}cm^{-2}$ achieved under a pure hydrogen atmosphere at 800 °C when used as SOFC anodes [Figure 3I]. Additionally, under a pure CO_2 atmosphere, the SF1.5M exhibited a high electrolytic current density of 1.2 $A{\cdot}cm^{-2}$ at a voltage of 1.4 V [Figure 3J][49]. It was evident that as the Fe content gradually increased, the performance of the SFM electrocatalyst improved. The results of O K-edge X-ray absorption spectroscopy showed that the enhancements of the electrochemical performance of SF1.5M were related to the enhancement of metal-oxygen hybridization [Figure 3K][49].

Transition metal ion doping SFM is also a strategy to enhance the electrocatalytic performance of SFM catalysts. The redox stability of the SFM matrix material was enhanced by doping the transition metal Mg into SFM, which was achieved by having the Fe ions in the driving SFM occupy two B-sites, resulting in a lattice structure denoted as $Sr_2(Mg_{1/3}Fe_{2/3})(Mo_{2/3}Fe_{1/3})O_6$ (SFMM) [Figure 4A][31,32]. The introduction of Mg was considered a beneficial enhancement for the redox stability of the SFM matrix material. The findings from the high-temperature XRD analysis supported the aforementioned claims [Figure 4B]. Specifically, under an inert atmosphere, the temperature-dependent behavior of SFMM revealed a transition from a tetragonal crystal structure to a cubic lattice structure, which led to an enhancement in the crystal's symmetry. Notably, no splitting of the diffraction peak was observed in high-temperature XRD, indicating the stability of the SFMM at high temperatures. Figure 4C shows the change of the total resistance of the SFMM with time under alternating cycles of redox atmosphere. The obtained resistivity data demonstrated good reproducibility and further supported the stability and reliability of SFMM in different gas environments[32]. In addition to exhibiting preeminent redox stability, SFMM demonstrated superior electrochemical performance, which achieved remarkable power densities of 531, 803, 1,038, and 1,316 $mW{\cdot}cm^{-2}$ when operated in a pure hydrogen atmosphere at temperatures of 750, 800, 850, and 900 °C, respectively [Figure 4D][32]. Based on the previous results, it had been demonstrated that the enhanced electrocatalytic performance of SFMM can be attributed to the doping of Mg, which lacks d-electrons. The doping of Mg led to a reduction in the coupling of the d-p band and the formation of a range of ADs, which facilitated the generation of oxygen vacancies[31,112]. The CO_2 absorption signal of the reduced SFMM sample was examined using *in-situ* infrared spectroscopy over a temperature range of 200-700 °C [Figure 4E]. The doping of Mg resulted in a distinct infrared band, indicating a significant increase in the adsorption capacity of SFMM. The Mg doping led to the formation of new adsorption sites, which was confirmed by this observation[31,112]. During CO_2 electrolysis at 800 °C, the SFMM-R (SFMM-reduce) cathode exhibited an electrolysis current density nearly twice that of SFM-R (SFM-reduce) [Figure 4F][31]. Hence, the introduction of elements lacking d electrons into DP structures presented a potentially efficacious strategy for augmenting their catalytic performance[31,112].

Hence, the preferred B-site doping element is Mg, which reduced the d-p band coupling to increase the catalytic activity of SFM for CO_2 and hydrogen[31]. The Mg doping enhances the redox stability of SFM and can intrinsically regulate its electronic structure. In addition, the doping of active transition metals can easily lead to the occurrence of *in-situ* exsolution. Improving the redox stability of SFM through the regulation of B-site transition metal ions remains to be explored. There is no doubt that the B-site ion

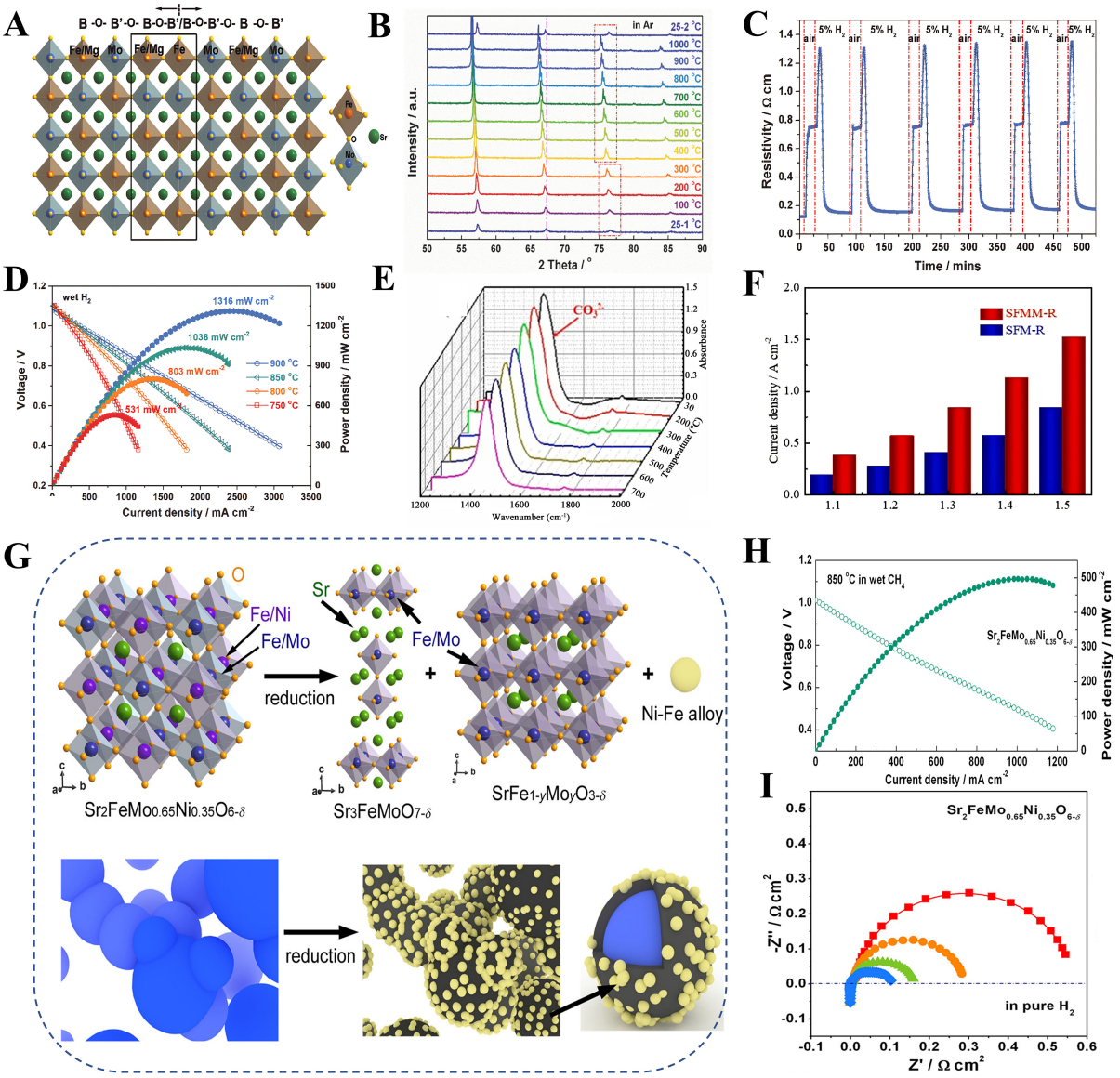

Figure 4. (A) Possible mechanisms of anti-site defects development in SFMM; (B) XRD of SFMM precursor at high temperatures from 25-1,000 °C in Argon; (C) SFMM redox cycling resistivity at 800 °C; (D) current voltage and related power density for single cell SFMM with 300 μm LSGM. Reproduced with permission[32], Copyright 2018, Wiley-VCH; (E) At an ambient temperature of 700 °C, *in-situ* infrared spectroscopy was used to investigate the adsorption of CO_2; (F) Comparison of current density produced with SOEC cathode prepared by SFM-R and SFMM-R at various applied potentials. Reproduced with permission[31], Copyright 2021, Elsevier; (G) Structure and surface morphology evolution models of SFMNi fuel electrode in H_2 atmosphere; (H) voltage and power density characteristics about the current density of a cell SFMNi/LDC/LSGM/LSCF with LSGM electrolyte support, operated under CH_4 conditions; (I) Nyquist points of impedance data from symmetrical cells SFMNi/LDC/LSGM/LDC/SFMNi measured in pure H_2 at different temperatures under open-circuit voltage. Reproduced with permission[37], Copyright 2016, American Chemical Society. SFMM: $Sr_2(Mg_{1/3}Fe_{2/3})(Mo_{2/3}Fe_{1/3})O_6$; XRD: X-ray diffraction; SOEC: solid oxide electrolysis cell; LSGM: $La_{0.2}Sr_{0.8}Ga_{0.8}Mg_{0.2}O_3$; SFM-R: Sr_2FeMoO_6-reduce; SFMM-R: $Sr_2(Mg_{1/3}Fe_{2/3})(Mo_{2/3}Fe_{1/3})O_6$-reduce; LDC: La doped ceria; LSCF: $La_{0.6}Sr_{0.4}Co_{0.2}Fe_{0.8}O_3$.

modulation of SFM is the most promising regulatory strategy. First of all, nearly 30 elements can be doped in the B-site, which indicates the regulatory strategies of B ions are very diverse. Secondly, the electron conduction of SFM needs to be achieved by the B-site active element. At the same time, the adsorption and activation sites of fuel gas are more concentrated in B-site active ions. Therefore, the regulation of the B-site ion of SFM holds significant importance in the application of SOC.

In-situ exsolution

In-situ exsolution is performed under SOC operating conditions, and the high temperature, reduction atmosphere, and electric potential drive induce the reconstruction of the crystal structure and the formation of oxygen vacancies. The formation of a large number of oxygen vacancies makes it easier for B-site transition metal ions to aggregate on the surface and pin to the oxide surface, thus forming a heterogeneous interface[5,113]. In the traditional surface modification method, due to the diversification of oxide surfaces, it is difficult for traditional surface modification methods to uniformly control the size and morphology of NPs. The weak adsorption between oxides and NPs brought about by traditional surface modification methods leads to unsatisfactory agglomeration of metal particles on the surface of the catalyst, resulting in a decrease in the activity of the catalyst[5,13,36,114]. Compared to traditional surface modification methods, *in-situ* exsolution enables more uniform and fine NPs to be anchored into the oxide surface. The alloy NPs embedded in the oxide have the characteristics of anti-agglomeration and high catalytic activity, which is also the reason for the high activity and stability of the SOC electrode regulated by *in-situ* exsolution.

The utilization of perovskite oxides as scaffolds enabled the incorporation of active transition metal ions into the perovskite oxide structure through oxidation conditions[93]. Subsequently, these ions can be exsolved *in-situ* under a reducing atmosphere, growing NPs on the oxide surface, which facilitated the anchoring of NPs that were more uniform and fine, eliminating the need for multiple complex steps, thereby significantly enhancing its performance. The SFM was transformed into a heterostructure of NPs and oxides by *in-situ* exsolution. The synergistic effect between the abundant oxygen vacancies in perovskite oxides and NPs was significant, thereby significantly improving the catalytic activity of SFM[93,115,116]. The latest research showed that it is possible to anchor the single Ru atoms on the metal oxide and apply it to the SOEC test by strong covalent metal-support interaction[117]. This may be a new direction for future SFM-related research to carry out SOC electrode modification at the atomic-scale level through the interface effect.

Due to the comparable ion radius and valence between Ni and Fe, the substitution of Ni for B-site ions in SFM was a common practice. Hence, the anode material $Sr_2FeMo_{0.65}Ni_{0.35}O_6$ (SFMNi) with high performance in SOFC was investigated. A schematic diagram illustrates the structural transformation and surface morphology evolution of SFMNi when subjected to a reducing atmosphere [Figure 4G][37]. Under the reduction conditions, the SFMNi underwent reduction, resulting in the formation of Ruddlesden-Popper (RP) phase Sr_3FeMoO_7 [a layered perovskite (LP)], while the internal structure of SFMNi remained as a DP. Additionally, Fe-Ni alloy NPs grew *in-situ* on the surface of oxide, leading to a significant enhancement in the electrochemical performance of electrocatalysts[37]. Furthermore, in the methane atmosphere at 850 °C, the power density of the SFMNi anode reached 500 $mW \cdot cm^{-2}$ [Figure 4H][37]. The electrochemical impedance spectrum of the SFMNi anode revealed its exceptional electrochemical performance. At temperatures of 700, 750, 800, and 850 °C, the anode exhibited impedances of 0.565, 0.290, 0.163, and 0.106 $\Omega \cdot cm^2$, respectively [Figure 4I][37].

Compared with SFM, SF1.5M had better redox stability[118,119]. Consequently, the introduction of doped transition metals into redox-stable SF1.5M maintained amazing structural stability while promoting the formation of metal-oxide heterogeneous interfaces on the surface of materials[118,119]. To better understand the whole process of *in-situ* exsolution, a series of advanced electrochemical *in-situ* characterization methods were used. Figure 5 illustrates the results obtained from *in-situ* TEM, which demonstrated the reversible nature of the phase transition of Co-Fe NPs under different atmospheres[120]. Specifically, Figure 6A depicts the schematic representation of the reversible phase transition under an oxidizing atmosphere and the growth of alloy NPs under a hydrogen atmosphere of Co-doped SF1.5M[120]. Figure 6B and C shows 12 redox stabilization and electrolysis tests performed on Co-doped SF1.5M for 200 h at

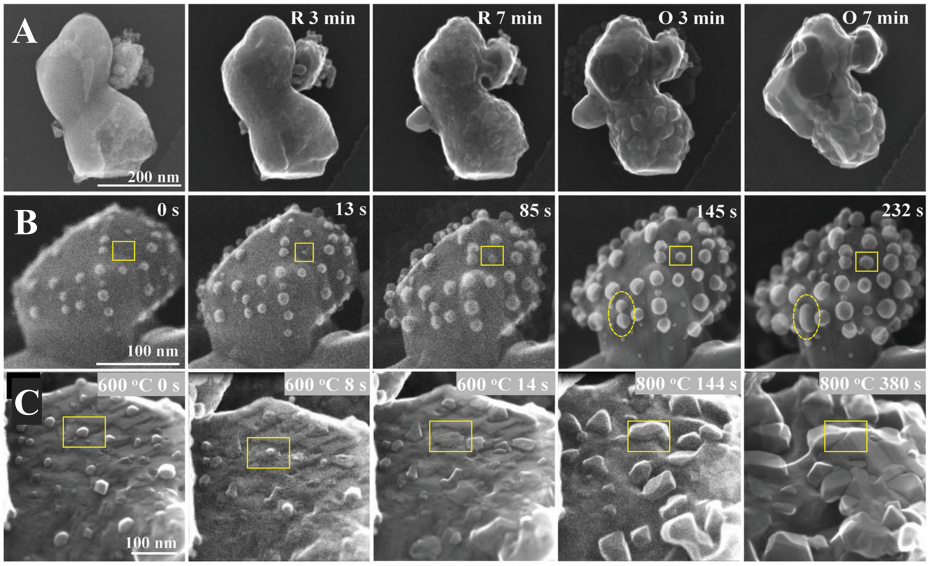

Figure 5. *in-situ* STEM images of Co-doped SF1.5M before and after reduction, after re-oxidation. (A) SEM images of a redox cycle at 800 °C; the R in the image is for reduction, and the O in the picture stands for oxidation; (B) photographs of a typical region in H_2 provided at 800 °C; and (C) images of a typical area in O_2 given at 600 °C, after that aggrandizing from 600 to 800 °C at rate of 5 °C·s^{-1} and remaining at 800 °C. Reproduced with permission[120], Copyright 2020, Wiley-VCH. STEM: Scanning transmission electron microscopy; SEM: scanning electron microscope.

800 °C. The excellent results illustrated the good stability of the metal-oxide heterogeneous interface of Co-doped SF1.5M, which was attributed to the strong synergy between the NPs and the oxide substrate[120].

Based on the aforementioned research findings, the strategy involving repeated redox operations of $Sr_2Fe_{1.4}Ru_{0.1}Mo_{0.5}O_6$ (SFRuM) had been proposed, aiming to enrich the surface of DP with a significant amount of Ru-Fe NPs through the dissolution and exsolution of Ru-Fe NPs[121]. *in-situ* XRD analysis revealed that, during the initial reduction stage, the diffraction peak intensity of the Ru-Fe alloy and its corresponding RP phase was weak [Figure 6D]. Subsequently, in the second reduction stage, the diffraction peak intensity of SFRuM was observed to weaken. The diffraction peak intensity of the corresponding Ru-Fe alloy and its corresponding RP phase was enhanced, which suggested that the repeated redox operations led to an increase of Ru-Fe alloy on the metal-oxide interface[121].

Figure 6E and F illustrates the remarkable electrochemical performance of SFRuM in SOEC cathodes during multiple redox operations. Notably, at an operating temperature and voltage of 800 °C and 1.2 V, respectively, the electrolytic CO_2 current density of SFRuM-R1 cells exhibited a 51.3% increase compared to SFRuM electrolysis cells without reduction[121]. Additionally, the electrolysis stability of the SFRuM-R2 electrolytic cell was assessed, demonstrating its exceptional ability to operate stably for 1,000 h. This confirms the stability of the NPs-oxide interface resulting from redox operations [Figure 6F][121] These findings have significant implications for CO_2 electrolysis, which can serve as a comprehensive strategy for improving the electrochemical performance of SOC through the process of *in-situ* exsolution[121].

The *in-situ* exsolution method of perovskites exhibits broad applicability across various domains, particularly in the context of CO_2RR. However, certain challenges persist, notably the inadequate stability of perovskites containing dissolved NPs at high voltage conditions, which significantly impeded their practical application[122,123]. Hence, the perovskite SFNM was utilized as a prototype to study the connection of

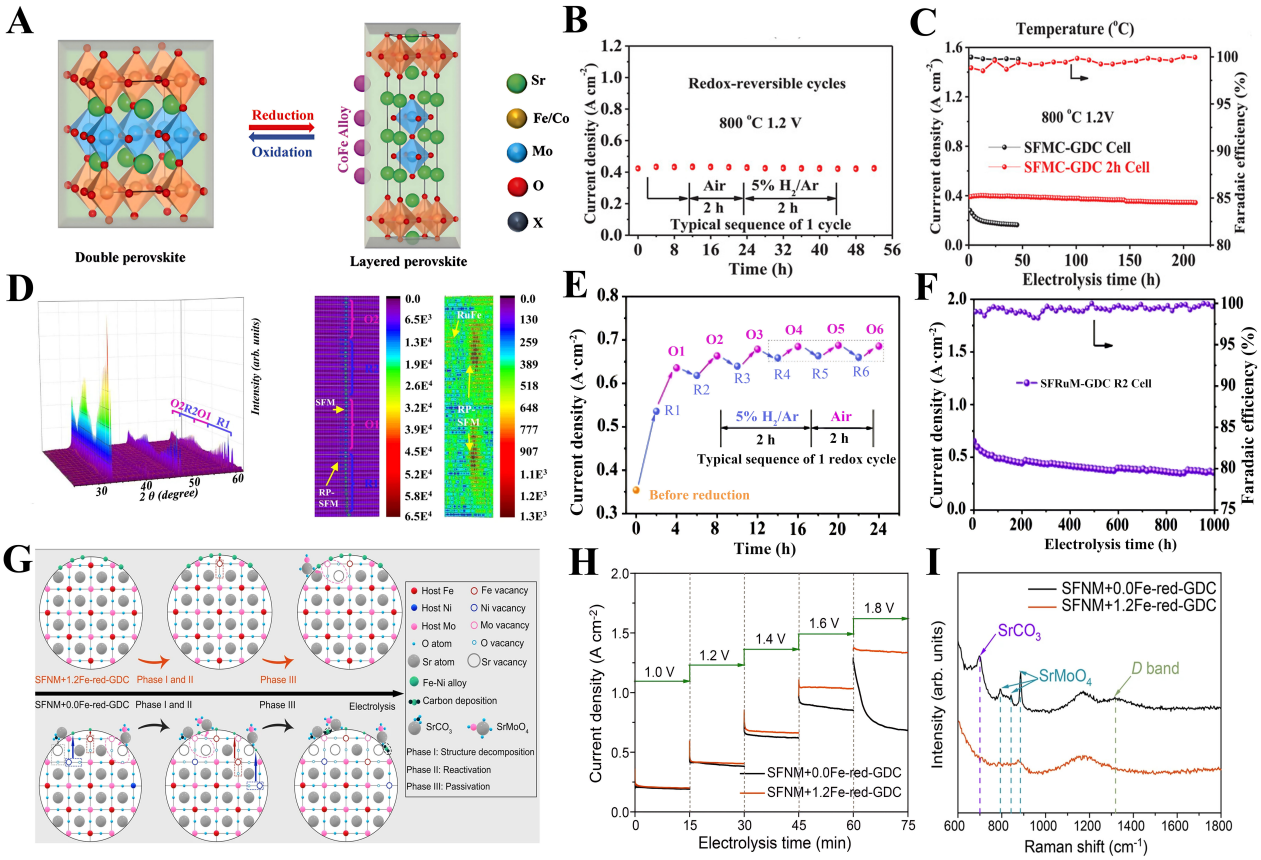

Figure 6. (A) The schematic diagram illustrates the *in-situ* exsolution and dissolution course of Co-doped SF1.5M; (B) The redox stability test of the Co-doped SF1.5M-GDC 2 h cell was evaluated at an operating voltage of 1.2 V and a temperature of 800 °C; (C) the stability test of Co-doped SF1.5M-GDC and Co-doped SF1.5M-GDC 2 h cell. Reproduced with permission[120], Copyright 2020, Wiley-VCH; (D) At 800 °C, *in-situ* XRD patterns of as-prepared SFRuM after switching between reducing and oxidizing atmospheres; (E) SFRuM-GDC cell CO_2 electrolysis performance after six redox cycles at 1.2 V and 800 °C; (F) At 800 °C and 1.2 V, the stability test of the SFRuM R2 cell and Faradaic efficiencies of CO were tested. Reproduced with permission[121], Copyright 2021, Springer Nature; (G) At high negative potentials, the processes of degradation caused by structural evolution; (H) The 15-min potential step chronoamperometry current density response curves; (I) Raman spectra were collected from the cathode surface of SFNM+0.0Fe-red-GDC and SFNM+1.2Fe-red-GDC after the long-term stability test. Reproduced with permission[124], Copyright 2022, Springer Nature. XRD: X-ray diffraction; SFRuM: $Sr_2Fe_{1.4}Ru_{0.1}Mo_{0.5}O_6$; GDC: Gd doped ceria.

structural changes and *in-situ* exsolution[108,124]. By using SFNM as a representative example, the impact of the evolution of the perovskite matrix structure on stability was elucidated. By introducing foreign Fe ions onto the perovskite surface, Zhang *et al.* completed the reversible regulation of perovskite phase transformation by controlling the reduction conditions[124,125]. The structural evolution process of SFNM supplemented with foreign Fe ions during the electrolysis of CO_2 was explained in Figure 6G[124]. Figure 6H presents the step-over-step amperometric measurement of the SFNM cathode, both with and without the introduction of foreign Fe ions, which suggested that SFNM supplemented with foreign Fe ions demonstrates favorable short-term stability at high voltage[124]. Furthermore, after subjecting SFNM to a long-term stability test lasting 100 h, it was evident from Figure 6I that SFNM, without the addition of foreign Fe ions, underwent surface alterations[124]. The presence of a segregating site, where $SrCO_3$ and $SrMoO_4$ compounds were formed, effectively inhibited the interaction between CO_2 and the active site, thereby impeding the process of CO_2 electrolysis[124]. However, the addition of foreign Fe ions to the SFNM catalyst effectively mitigates this issue, resulting in improved stability[124,126].

The strategy enabled control over the structural transformation of the primary perovskite phase from a DP to LP, while simultaneously controlling the dissolution and exsolution of alloy particles[124,125]. By optimizing the interface structure design of the perovskite surface, the important role of phase structure transition in the catalytic mechanism of perovskite can be better understood [Figure 7A][125]. The study revealed that the interface structure featuring DP-NPs exhibited the most pronounced catalytic activity. The interface structure comprising LP-NPs demonstrated superior stability, which contributed to a deeper comprehension of the catalytic reaction mechanism through the mechanism of *in-situ* exsolution [Figure 7B][125].

The DFT calculation was used to study the heterogeneous interface of CO_2 adsorption in different configurations of perovskite oxide SFNM-metal NPs. The CO_2 adsorption at V_o was the most stable on the surface of DP-V_o and LP-V_o without *in-situ* exsolution [Figure 7C]. LP-V_o showed stronger chemical adsorption of CO_2, and for the case involving *in-situ* exsolution of Fe-Ni alloy, CO_2 was more inclined to adsorb Fe-Ni clusters exsolved *in-situ* [Figure 7C][125]. Among them, the C atom was bonded with the Fe ion of the Fe-Ni cluster, and the CO_2 molecule was attached to the oxygen vacancy of the substrate [Figure 7C]. The DP-NPs model showed the strongest CO_2 adsorption capacity, with an E_{ad} of -2.81 eV, followed by the LP-NPs model, with an E_{ad} of -1.47 eV, and finally, the DLP-NPs (double perovskite and layered perovskite with exsolved nanoparticles) model with E_{ad} values of -1.04 and 0.54 eV [Figure 7C]. It was not difficult to see that the heterogeneous interface with pure DP substrate was generally stronger for CO_2 adsorption capacity, and on the heterogeneous interface with DLP mixed substrate, DP was also stronger for CO_2 adsorption capacity[125].

The SFM was transformed into a heterostructure of NPs and oxides by *in-situ* exsolution. The synergistic effect between the abundant oxygen vacancies in perovskite oxides and NPs was significant, thereby substantially improving the catalytic activity of SFM. The *in-situ* exsolution strategy is currently a research hotspot in the field of SOC. By combining the *in-situ* exsolution strategy with the B-site ion regulation strategy, the NPs-oxide heterogeneous interface can be formed *in-situ* under certain conditions. Compared with traditional impregnation methods, the SOC electrode obtained by the *in-situ* exsolution method has higher catalytic activity of SFM. The latest research showed that it is possible to anchor the single Ru atoms on the metal oxide and apply it to the SOEC test by strong covalent metal-support interaction. This may be a new direction for future SFM-related research to carry out SOC electrode modification at the atomic-scale level through the interface effect. Interface can be formed *in-situ* under certain conditions. Compared with traditional impregnation methods, the SOC electrode obtained by the *in-situ* exsolution method has higher activity and stability while saving costs. However, the structure and mechanism formation process related to *in-situ* exsolution still needs to be explored urgently. Fe is more easily dissolved *in-situ* in combination with catalytically active transition metal cations (e.g., Ni, Co, Ru, and Cu). When Ru was doped with SF1.5M for CO_2RR, the interface between the dissolved Ru-Fe alloy and the perovskite showed high stability and activity[121]. Meanwhile, the combination of Ni and Fe to form an *in-situ* exsolution has also attracted extensive attention. The boundary between *in-situ* exsolution and structural stability, that is, the extent to which active transition metal ion doping contributes to *in-situ* exsolution, warrants further investigation. In addition, the concept of *in-situ* exsolution is still underexplored. Current research focuses on how *in-situ* exsolution can improve the performance of SOC. However, the boundary between *in-situ* exsolution and element doping remains a subject requiring exploration, that is, how to determine the doping ratio of active transition metals and weigh the relationship between the structure of the electrode surface interface and the improvement of the intrinsic electronic structure of the material is crucial. This area may also be the direction of future research.

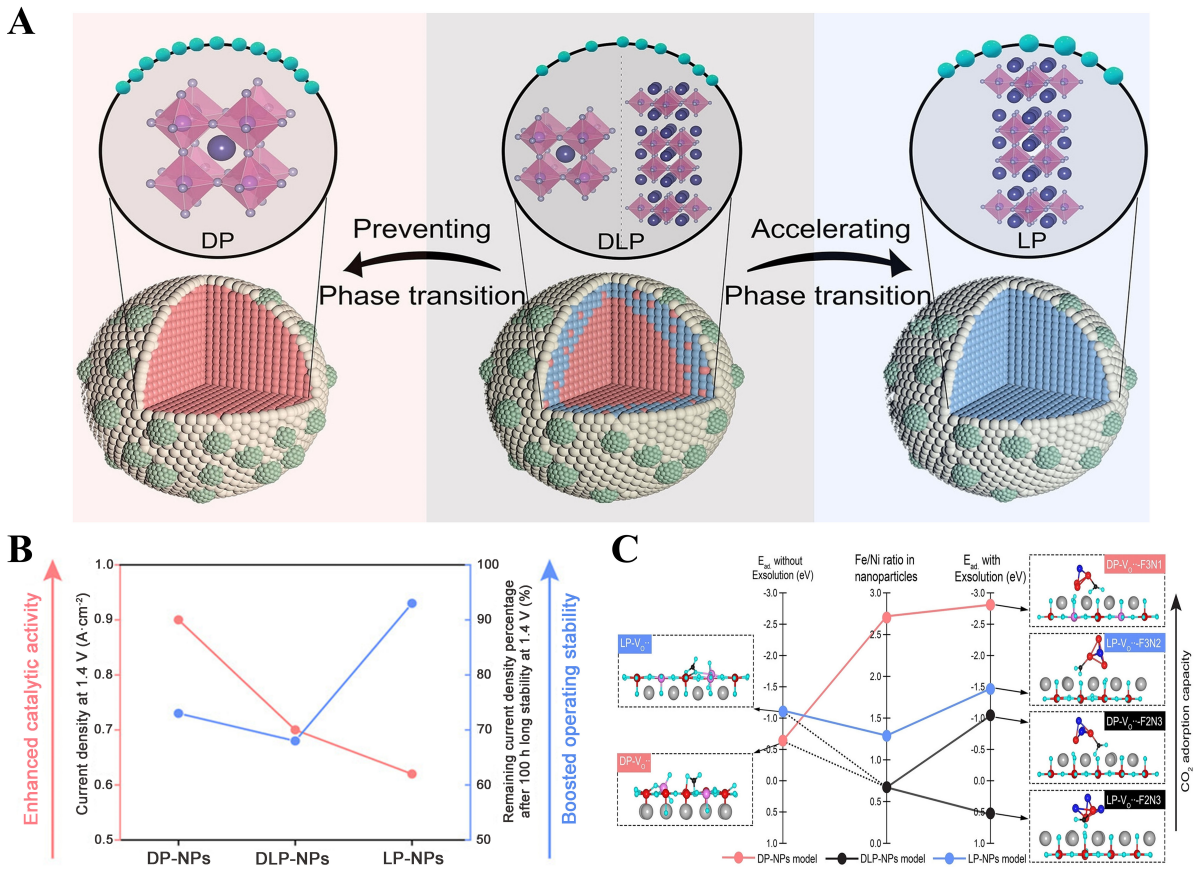

Figure 7. (A) Design strategy for exsolution-facilitated perovskite-exsolved NPs based on SFNM with pure DP phase, pure LP phase, and DLP scaffolds. (In the schematic models, the red area is the DP structure, the blue area is the LP structure, and the light green area is the Fe-Ni NPs. Purple spheres in 2D models are Sr atoms, pink spheres are Fe/Ni/Mo atoms, gray spheres are oxygen atoms, and green spheres are exsolved Fe-Ni alloy NPs); (B) Changes in phase structure cause a shift in the activity and stability of perovskite oxides; (C) DFT calculation of carbon dioxide adsorption configurations and adsorption energies on the surface of DP-V_o, LP-V_o, DP-V_o-F2N3, DP-V_o-F3N1, LP-V_o-F2N3, LP-V_o-F3N2 models, in the above models, the grey balls are Sr atoms, the red balls are Fe atoms, the dark blue balls are Ni atoms, the pink balls are Mo atoms, and the light blue balls are O atoms. Reproduced with permission[125], Copyright 2023, Wiley-VCH. NPs: Nanoparticles; SFNM: $Sr_2Fe_{1.3}Ni_{0.2}Mo_{0.5}O_6$; DP: double perovskite; LP: layered perovskite; DLP: double perovskite and layered perovskite; DFT: density functional theory.

Within the SOC segment, the main methods of regulating electrocatalysts based on elemental doping are A-site ions regulation, B-site ions regulation, and *in-situ* exsolution strategy [Figure 8]. At present, the research mainly focuses on the regulation of the effects of A and B ions on the crystal and electronic structure of SFM electrocatalysts. The beneficial effects of crystal structure and electronic structure change on electrochemical performance are highlighted. The relationship between crystal/electronic structure and electrochemical performance is effectively constructed. However, given the variety of perovskite oxides, it is critical to uncover the relationship between the performance and parameters of SFM-based catalysts, and it is possible to propose descriptors that can specifically describe the activity of SFM-based electrodes to guide the prediction of new materials with higher efficiency, thereby avoiding long experimental cycles, which may be the trend of material design in the era of artificial intelligence.

CHALLENGES AND OUTLOOK

Despite the wide use of SFM-based electrocatalysts in SOC electrodes owing to their high performance, there are still some challenges regarding the synthesis, modulation and application of SFM-based electrocatalysts.

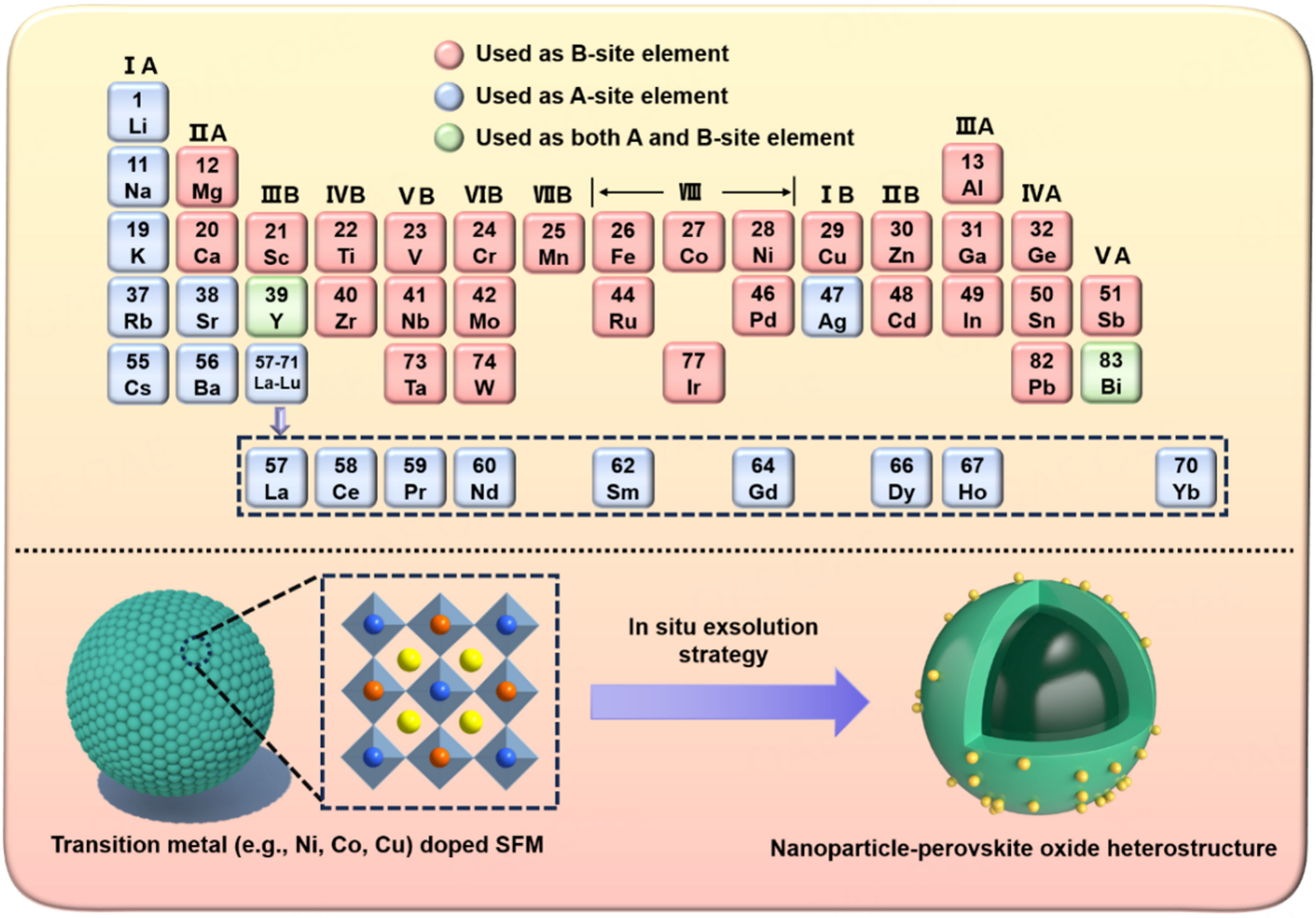

Figure 8. Summary of SFM main modulation methods. SFM: Sr_2FeMoO_6.

Most studies modulate the magnetic properties of SFM by regulating the synthesis conditions. Conversely, a limited amount of research is dedicated to exploring the preparation of SFM specifically for catalytic applications. Selecting appropriate preparation methods, synthesizing high-purity SFM-based catalysts applied to electrocatalysis, studying the influence of different preparation methods on the physical and chemical properties of SFM-based electrocatalysts, and then elucidating the relationship between synthesis and performance may be one of the essential directions of SFM catalyst synthesis in the future.

The main strategies to regulate the activity of SFM-based electrocatalysts are A/B site modulation and *in-situ* exsolution. The ion substitution strategy can regulate the intrinsic structure of SFM, but the intrinsic relationship between the structure and the electrocatalytic activity of SFM needs to be investigated. A clear understanding of the structure-activity relationship of SFM is the basis for improving its electrocatalytic activity. At present, extensive research has been conducted on the *in-situ* exsolution of SFM-based electrocatalysts. The enhancement of catalytic activity and stability of these electrocatalysts can be achieved by constructing heterojunctions via *in-situ* exsolution. Nevertheless, owing to the intricate nature of nano-heterostructures, numerous obstacles arise. The intricate nature of their formation process often surpasses the existing model. Therefore, it is necessary to comprehensively study the whole process of *in-situ* exsolution and dissolution, and the *in-situ* exsolution process involves the nucleation and growth of grains; considering the impact of grain nucleation and growth on the interface effect of electrocatalyst surface, it is necessary to study the mechanism of *in-situ* exsolution more thoroughly.

Ultimately, by comprehending the whole process of *in-situ* exsolution, it becomes possible to exert improved control over the surface morphology of SFM-based electrocatalysts through the manipulation of experimental conditions and preparation methods. Additionally, the utilization of more *in-situ* and real-time electrochemical characterization methods enables the identification of rate-limiting steps and catalytic reactions occurring on the surface of SOC electrodes[127]. Establishing the relationship between electrode performance and structure and influencing the electrocatalytic activity of electrocatalysts through precise structure and surface interface regulation may be the desired goal.

Furthermore, SFM, a perovskite oxide exhibiting giant magnetoresistance at room temperature, has found extensive applications in the realm of spintronics[50]. Regrettably, there is a dearth of studies exploring the relationship between magnetism and electrocatalysis, specifically the influence of particle spin on the electrocatalytic reaction pathway[128,129]. It has been shown that it is feasible to improve the electrocatalytic activity of SFM through spin regulation based on the spin-orbit coupling exchange interaction of ferromagnetic materials[130,131]. Hence, the correlation between spin and electrocatalysis has the potential to provide insights into the development of catalysts based on SFM.

Due to its magnetic and catalytic properties, SFM has attracted much attention in the field of spintronics and electrochemistry and has a good application prospect. However, from laboratory scale to industrial scale production, there will inevitably be problems, such as the mismatch of thermal expansion coefficients, the poor life of the stack, and the degradation of performance after the increase of cell area, which may be the basis for SFM-based catalysts to have a broader future.

In addition, SFM has excellent ionic conductivity, which may be the basis for potential applications for solid-state gas sensors and gas separation membranes. Although SFM cannot be stabilized under air, the stability of SFM in air and the concentration of oxygen vacancies can be controlled by atomic substitution, which can be better used in sensors and gas separation membranes. Compared with the proton conductor, the oxygen ion has a larger radius and higher activation energy. Therefore, the oxygen ion conductor applied to SOEC needs to operate at high temperatures. While the activation energy of proton conductors is low, limited by their low stability in the environment containing CO_2 and H_2O, the research on SOEC is more focused on oxygen ion conductors. In the future, SFM with high oxygen ion conduction performance may be more used in SOEC devices.

Numerous scholarly investigations on the regulation of electrocatalysts in SOC electrodes have been published, and the vast majority of these studies are based on experimental phenomena. In recent years, with the rapid development of artificial intelligence and first-principles computing, it is important to obtain potential information that may be hidden in existing data sets through data-driven methods, making it possible to use theoretical knowledge and information science and techniques to guide the design of SOC electrocatalysts. Consequently, the utilization of machine learning methods for the screening of SOC electrode materials holds considerable potential[132,133]. Currently, the machine learning approach has been employed to characterize the kinetic reaction rate of perovskite-related oxides at elevated temperatures, which utilizes the ionic Lewis acid strength descriptor[133]. Hence, the identification of crucial catalytic activity descriptors and the subsequent design and development of high-performance SOC electrodes using machine learning-driven approaches pose a novel and significant undertaking.

CONCLUSION

The advancements of SFM catalysts for SOCs are summarized in this review, focusing on the synthesis, modulation, and application. It is found that different preparation methods affect the physicochemical

properties of SFM electrocatalysts, especially the ADs and oxygen vacancy concentrations, which are closely related to the catalytic activity of SFM. It is necessary to take into consideration the effects of various preparation methods on SFM electrocatalysts. A/B site doping, surface modulation, and *in-situ* exsolution are the main ways of regulating. Compared with surface modification and element doping, *in-situ* exsolution can better regulate the catalytic activity and stability. Surface modification is often referred to as impregnation/infiltration, and while better electrochemical performance can be achieved by infiltrating metals onto the electrode surface using the wet chemistry method, the potential for insufficient stability remains. At high temperatures, the sintering or agglomeration of metal catalysts reduces the density of active sites and the performance of SOC. Surface modification often requires complex processes and instrumentation, which means high costs and is not conducive to the spread of large-scale manufacturing. The traditional element doping regulates the intrinsic structure of the material through the substitution of atoms, while the *in-situ* exsolution generated by the element doping can produce anti-agglomeration NPs, which are embedded on the surface of perovskite in the form of NPs to form a NPs-oxide heterogeneous interface, which maintains excellent stability and activity under SOC operating conditions.

Although substantial progress has been made using these regulation methods separately, the rational design of the SFM structure combining these approaches remains an urgent issue. The main reason lies in the fact that the relationship between the performance and structure of SFM-based catalysts is still unknown due to the diversity of modified SFM structures. Advanced tools such as artificial intelligence are needed to solve these problems. The applications of SFM catalysts in electrocatalysis have great potential for industrial applications. However, compared to conventional Ni-based electrodes, there are still some challenges due to insufficient activity and poor stability. In order to improve the catalytic activity of the SFM catalyst and promote its application in SOC, it is necessary to control its crystal and electronic structure, deepen the understanding of the catalytic mechanism, and optimize its surface and interface design. This review provides a scientific basis for the guidance of the synthesis, modulation, and application of SFM.

DECLARATIONS

Authors' contributions

Designed, prepared and revised the manuscript: Liao Y, Liu J, Luo JL
All authors contributed to the discussion and preparation of the manuscript.

Availability of data and materials

Not applicable.

Financial support and sponsorship

This work was supported by the National Natural Science Foundation of China (No. 22272108; No. 21975163), Shenzhen Science and Technology Program (No. KQTD20190929173914967; No. JCYJ20220531102408019; No. JCYJ20200109110416441; No. ZDSYS2022052717 1401003), and the Start-up Funds for Young Teachers of Shenzhen University (No. 000001032103).

Conflicts of interest

All authors declared that there are no conflicts of interest.

Ethical approval and consent to participate

Not applicable.

Consent for publication

Not applicable.

REFERENCES

1. Gür TM. Carbon dioxide emissions, capture, storage and utilization: review of materials, processes and technologies. *Prog Energy Combust Sci* 2022;89:100965. DOI
2. Pan X, Shao T, Zheng X, Zhang Y, Ma X, Zhang Q. Energy and sustainable development nexus: a review. *Energy Strategy Rev* 2023;47:101078. DOI
3. Li W, Luo J. High-temperature electrochemical devices based on dense ceramic membranes for CO_2 conversion and utilization. *Electrochem Energ Rev* 2021;4:518-44. DOI
4. Li Y, Zhang W, Zheng Y, et al. Controlling cation segregation in perovskite-based electrodes for high electro-catalytic activity and durability. *Chem Soc Rev* 2017;46:6345-78. DOI
5. Cao J, Ji Y, Shao Z. Nanotechnologies in ceramic electrochemical cells. *Chem Soc Rev* 2024;53:450-501. DOI
6. Wang W, Su C, Wu Y, Ran R, Shao Z. Progress in solid oxide fuel cells with nickel-based anodes operating on methane and related fuels. *Chem Rev* 2013;113:8104-51. DOI
7. Si F, Liu S, Liang Y, Fu X, Zhang J, Luo J. Fuel cell reactors for the clean cogeneration of electrical energy and value-added chemicals. *Electrochem Energy Rev* 2022;5:25. DOI
8. Zhang W, Hu X, Zhou Y, et al. A solid oxide fuel cell runs on hydrocarbon fuels with exceptional durability and power output. *Adv Energy Mater* 2022;12:2202928. DOI
9. Song Y, Zhang X, Xie K, Wang G, Bao X. High-temperature CO_2 electrolysis in solid oxide electrolysis cells: developments, challenges, and prospects. *Adv Mater* 2019;31:1902033. DOI PubMed
10. Boldrin P, Brandon NP. Progress and outlook for solid oxide fuel cells for transportation applications. *Nat Catal* 2019;2:571-7. DOI
11. Cao J, Ji Y, Shao Z. Perovskites for protonic ceramic fuel cells: a review. *Energy Environ Sci* 2022;15:2200-32. DOI
12. Cheng Z, Wang J, Choi Y, Yang L, Lin MC, Liu M. From Ni-YSZ to sulfur-tolerant anode materials for SOFCs: electrochemical behavior, in situ characterization, modeling, and future perspectives. *Energy Environ Sci* 2011;4:4380. DOI
13. Connor PA, Yue X, Savaniu CD, et al. Tailoring SOFC electrode microstructures for improved performance. *Adv Energy Mater* 2018;8:1800120. DOI
14. Wang JH, Cheng Z, Brédas JL, Liu M. Electronic and vibrational properties of nickel sulfides from first principles. *J Chem Phys* 2007;127:214705. DOI PubMed
15. Gong M, Liu X, Trembly J, Johnson C. Sulfur-tolerant anode materials for solid oxide fuel cell application. *J Power Sources* 2007;168:289-98. DOI
16. Yang L, Cheng Z, Liu M, Wilson L. New insights into sulfur poisoning behavior of Ni-YSZ anode from long-term operation of anode-supported SOFCs. *Energy Environ Sci* 2010;3:1804-9. DOI
17. Boldrin P, Ruiz-Trejo E, Mermelstein J, Bermúdez Menéndez JM, Ramı Rez Reina T, Brandon NP. Strategies for carbon and sulfur tolerant solid oxide fuel cell materials, incorporating lessons from heterogeneous catalysis. *Chem Rev* 2016;116:13633-84. DOI PubMed
18. Li Y, Zhan Z, Xia C. Highly efficient electrolysis of pure CO_2 with symmetrical nanostructured perovskite electrodes. *Catal Sci Technol* 2018;8:980-4. DOI
19. Wang Z, Tian Y, Li Y. Direct CH4 fuel cell using Sr_2FeMoO_6 as an anode material. *J Power Sources* 2011;196:6104-9. DOI
20. Cernea M, Vasiliu F, Bartha C, Plapcianu C, Mercioniu I. Characterization of ferromagnetic double perovskite Sr_2FeMoO_6 prepared by various methods. *Ceram Int* 2014;40:11601-9. DOI
21. Cernea M, Vasiliu F, Plapcianu C, et al. Preparation by sol-gel and solid state reaction methods and properties investigation of double perovskite Sr_2FeMoO_6. *J Eur Ceram Soc* 2013;33:2483-90. DOI
22. Rager J, Zipperle M, Sharma A, Macmanus-Driscoll JL. Oxygen stoichiometry in Sr_2FeMoO_6, the determination of Fe and Mo valence states, and the chemical phase diagram of SrO-Fe_3O_4-MoO_3. *J Am Ceram Soc* 2004;87:1330-5. DOI
23. Farzin YA, Babaei A, Ataie A. Low-temperature synthesis of Sr_2FeMoO_6 double perovskite; structure, morphology, and magnetic properties. *Ceram Int* 2020;46:16867-78. DOI
24. Das R, Chaudhuri U, Mahendiran R. Microwave magnetoresistance and microwave absorption in Sr_2FeMoO_6. *ACS Appl Electron Mater* 2021;3:3072-8. DOI
25. Zhai Y, Qiao J, Huo G, Han S. Synthesis, magnetic and electrical transport properties of magnetoresistance material Sr_2FeMoO_6 by microwave sintering. *J Magn Magn Mater* 2012;324:2006-10. DOI
26. Li XY, Yao ZF, Zhang LY, Zheng GH, Dai ZX, Chen KY. Generation of oxygen vacancies on Sr_2FeMoO_6 to improve its photocatalytic performance through a novel preparation method involving pH adjustment and use of surfactant. *Appl Surf Sci* 2019;480:262-75. DOI

27. Mami A, Boukhachem A, Mellouki I, Amlouk M. Synthesis and physical characterization of Sr_2FeMoO_6 and Sr_3FeMoO_7 thin films. *Mater Lett* 2019;243:77-80. DOI
28. Valdés J, Reséndiz D, Cuán Á, et al. Sol-gel synthesis of the double perovskite Sr_2FeMoO_6 by microwave technique. *Material* 2021;14:3876. DOI PubMed PMC
29. Kumar A, Dutta S, Kim S, et al. Solid-state reaction synthesis of nanoscale materials: strategies and applications. *Chem Rev* 2022;122:12748-863. DOI
30. Raittila J, Salminen T, Suominen T, Schlesier K, Paturi P. Nanocrystalline Sr_2FeMoO_6 prepared by citrate-gel method. *J Phys Chem Solids* 2006;67:1712-8. DOI
31. Xi X, Liu J, Fan Y, et al. Reducing d-p band coupling to enhance CO_2 electrocatalytic activity by Mg-doping in $Sr_2FeMoO_{6-\delta}$ double perovskite for high performance solid oxide electrolysis cells. *Nano Energy* 2021;82:105707. DOI
32. Du Z, Zhao H, Li S, et al. Exceptionally high performance anode material based on lattice structure decorated double perovskite $Sr_2FeMo_{2/3}Mg_{1/3}O_{6-\delta}$ for solid oxide fuel cells. *Adv Energy Mater* 2018;8:1800062. DOI
33. Das R, Choudhary RNP, Pradhan D. Structural and electrical characteristics of double perovskite: Sr_2FeMoO_6. *Mater Sci Eng B* 2022;281:115715. DOI
34. Wang J, Kumar A, Wardini JL, et al. Exsolution-driven surface transformation in the host oxide. *Nano Lett* 2022;22:5401-8. DOI
35. Kousi K, Tang C, Metcalfe IS, Neagu D. Emergence and future of exsolved materials. *Small* 2021;17:e2006479. DOI PubMed
36. Ding D, Li X, Lai SY, Gerdes K, Liu M. Enhancing SOFC cathode performance by surface modification through infiltration. *Energy Environ Sci* 2014;7:552-75. DOI
37. Du Z, Zhao H, Yi S, et al. High-performance anode material $Sr_2FeMo_{0.65}Ni_{0.35}O_{6-\delta}$ with *in situ* exsolved nanoparticle catalyst. *ACS Nano* 2016;10:8660-9. DOI PubMed
38. Xi X, Fan Y, Zhang J, Luo J, Fu X. *In situ* construction of hetero-structured perovskite composites with exsolved Fe and Cu metallic nanoparticles as efficient CO_2 reduction electrocatalysts for high performance solid oxide electrolysis cells. *J Mater Chem A* 2022;10:2509-18. DOI
39. Yang M, Yao Z, Liu S, et al. Bismuth doped $Sr_2Fe_{1.5}Mo_{0.5}O_{6-\delta}$ double perovskite as a robust fuel electrode in ceramic oxide cells for direct CO_2 electrolysis. *J Mater Sci Technol* 2023;164:160-7. DOI
40. Muñoz-García AB, Pavone M. K-doped $Sr_2Fe_{1.5}Mo_{0.5}O_{6-\delta}$ predicted as a bifunctional catalyst for air electrodes in proton-conducting solid oxide electrochemical cells. *J Mater Chem A* 2017;5:12735-9. DOI
41. Muñoz-García AB, Pavone M, Carter EA. Effect of antisite defects on the formation of oxygen vacancies in Sr_2FeMoO_6: implications for ion and electron transport. *Chem Mater* 2011;23:4525-36. DOI
42. Reyes AM, Arredondo Y, Navarro O. Effect of cationic disorder on the magnetic moment of Sr_2FeMoO_6: ab initio calculations. *J Phys Chem C* 2016;120:4048-52. DOI
43. Mishra R, Restrepo OD, Woodward PM, Windl W. First-principles study of defective and nonstoichiometric Sr_2FeMoO_6. *Chem Mater* 2010;22:6092-102. DOI
44. Sunarso J, Hashim SS, Zhu N, Zhou W. Perovskite oxides applications in high temperature oxygen separation, solid oxide fuel cell and membrane reactor: a review. *Prog Energy Combust Sci* 2017;61:57-77. DOI
45. Yin W, Weng B, Ge J, Sun Q, Li Z, Yan Y. Oxide perovskites, double perovskites and derivatives for electrocatalysis, photocatalysis, and photovoltaics. *Energy Environ Sci* 2019;12:442-62. DOI
46. Kozuka H, Ohbayashi K, Koumoto K. Electronic conduction in La-based perovskite-type oxides. *Sci Technol Adv Mater* 2015;16:026001. DOI PubMed PMC
47. Bartha C, Plapcianu C, Crisan A, Enculescu M, Leca A. Structural and magnetic properties of Sr_2FeMoO_6 obtained at low temperatures. Available from: https://www.chalcogen.ro/773_BarthaC.pdf. [Last accessed on 21 Feb 2024].
48. Saloaro M, Hoffmann M, Adeagbo WA, et al. Toward versatile Sr_2FeMoO_6-based spintronics by exploiting nanoscale defects. *ACS Appl Mater Interfaces* 2016;8:20440-7. DOI PubMed
49. Xi X, Liu J, Luo W, et al. Unraveling the enhanced kinetics of $Sr_2Fe_{1+x}Mo_{1-x}O_{6-\delta}$ electrocatalysts for high-performance solid oxide cells. *Adv Energy Mater* 2021;11:2102845. DOI
50. Kobayashi KI, Kimura T, Sawada H, Terakura K, Tokura Y. Room-temperature magnetoresistance in an oxide material with an ordered double-perovskite structure. *Nature* 1998;395:677-680. DOI
51. Phuyal D, Mukherjee S, Panda SK, et al. Nonlocal interactions in the double perovskite Sr_2FeMoO_6 from core-level X-ray spectroscopy. *J Phys Chem C* 2021;125:11249-56. DOI
52. Varma A, Mukasyan AS, Rogachev AS, Manukyan KV. Solution combustion synthesis of nanoscale materials. *Chem Rev* 2016;116:14493-586. DOI PubMed
53. Feinle A, Elsaesser MS, Hüsing N. Sol-gel synthesis of monolithic materials with hierarchical porosity. *Chem Soc Rev* 2016;45:3377-99. DOI PubMed
54. Li C, Cailei Y, Junmin X, Wang J. Mechanically activated synthesis and magnetoresistance of nanocrystalline double perovskite Sr_2FeMoO_6. *J Am Ceram Soc* 2005;88:2635-8. DOI
55. Martynczuk J, Arnold M, Wang H, Caro J, Feldhoff A. How $(Ba_{0.5}Sr_{0.5})(Fe_{0.8}Zn_{0.2})O_{3-\delta}$ and $(Ba_{0.5}Sr_{0.5})(Co_{0.8}Fe_{0.2})O_{3-\delta}$ perovskites form via an EDTA/citric acid complexing method. *Adv Mater* 2007;19:2134-40. DOI
56. Hu Y, Sun Y, Wang X. Effect of gas flow rate on transport properties of Sr_2FeMoO_6. *J Magn Magn Mater* 2022;553:169234. DOI
57. Angervo I, Saloaro M, Tikkanen J, Huhtinen H, Paturi P. Improving the surface structure of high quality Sr_2FeMoO_6 thin films for

multilayer structures. *Appl Surf Sci* 2017;396:754-9. DOI

58. Jacobo SE. Novel method of synthesis for double-perovskite Sr_2FeMoO_6. *J Mater Sci* 2005;40:417-21. DOI
59. Takeda T, Ito M, Kikkawa S. Preparation of magneto-resistive Sr_2FeMoO_6 through molybdic acid gelation. *J Alloys Compd* 2008;449:93-5. DOI
60. E P, Zhang JS, Yao LD, et al. The structural and electrical properties of nano-scale Sr_2FeMoO_6 under high pressures. *J Mater Sci* 2006;41:7374-9. DOI
61. Yang D, Yang T, Sun Q, Chen Y, Lampronti GI. The annealing effects on the crystal structure, magnetism and microstructure of the ferromagnetic double perovskite Sr_2FeMoO_6 synthesized via spark plasma sintering. *J Alloys Compd* 2017;728:337-42. DOI
62. Yang CW, Fang TT. Structures and development mechanism of the anti-phase boundaries in Sr_2FeMoO_6. *J Electrochem Soc* 2012;159:P35. DOI
63. Taylor DD, Schreiber NJ, Brown CM, Arevalo-Lopez AM, Rodriguez EE. Stabilization of cubic Sr_2FeMoO_6 through topochemical reduction. *Chem Commun* 2015;51:12201-4. DOI PubMed
64. Wang K, Sui Y. Influence of the modulating interfacial state on Sr_2FeMoO_6 powder magnetoresistance properties. *Solid State Commun* 2004;129:135-8. DOI
65. Zhang L, Zhou Q, He Q, He T. Double-perovskites $A_2FeMoO_{6-\delta}$ (A = Ca, Sr, Ba) as anodes for solid oxide fuel cells. *J Power Sources* 2010;195:6356-66. DOI
66. Huan Y, Li Y, Yin B, Ding D, Wei T. High conductive and long-term phase stable anode materials for SOFCs: A_2FeMoO_6 (A = Ca, Sr, Ba). *J Power Sources* 2017;359:384-90. DOI
67. Xi X, Cao Z, Shen X, et al. In situ embedding of CoFe nanocatalysts into Sr_3FeMoO_7 matrix as high-performance anode materials for solid oxide fuel cells. *J Power Sources* 2020;459:228071. DOI
68. Liu Q, Dong X, Xiao G, Zhao F, Chen F. A novel electrode material for symmetrical SOFCs. *Adv Mater* 2010;22:5478-82. DOI
69. Liu Q, Yang C, Dong X, Chen F. Perovskite $Sr_2Fe_{1.5}Mo_{0.5}O_{6-\delta}$ as electrode materials for symmetrical solid oxide electrolysis cells. *Int J Hydrogen Energy* 2010;35:10039-44. DOI
70. Liu Q, Bugaris DE, Xiao G, et al. $Sr_2Fe_{1.5}Mo_{0.5}O_{6-\delta}$ as a regenerative anode for solid oxide fuel cells. *J Power Sources* 2011;196:9148-53. DOI
71. Zheng Y, Chen Z, Zhang J. Solid oxide electrolysis of H_2O and CO_2 to produce hydrogen and low-carbon fuels. *Electrochem Energ Rev* 2021;4:508-17. DOI
72. Fabbri E, Nachtegaal M, Binninger T, et al. Dynamic surface self-reconstruction is the key of highly active perovskite nano-electrocatalysts for water splitting. *Nat Mater* 2017;16:925-31. DOI
73. Long X, Zhao B, Zhao Q, et al. Ru-RuO_2 nano-heterostructures stabilized by the sacrificing oxidation strategy of Mn_3O_4 substrate for boosting acidic oxygen evolution reaction. *Appl Catal B Environ* 2024;343:123559. DOI
74. Chen H, Liu J, Wu X, et al. Pt-Co electrocatalysts: syntheses, morphologies, and applications. *Small* 2022;18:e2204100. DOI PubMed
75. Chen H, Wu X, Liu D, et al. Highly efficient C@Ni-Pd bifunctional electrocatalyst for energy-saving hydrogen evolution and value-added chemicals co-production from ethanol aqueous solution. *Chem Eng J* 2023;474:145639. DOI
76. Tomar AK, Pan UN, Kim NH, Lee JH. Enabling lattice oxygen participation in a triple perovskite oxide electrocatalyst for the oxygen evolution reaction. *ACS Energy Lett* 2023;8:565-73. DOI
77. Zhu K, Wu T, Li M, Lu R, Zhu X, Yang W. Perovskites decorated with oxygen vacancies and Fe-Ni alloy nanoparticles as high-efficiency electrocatalysts for the oxygen evolution reaction. *J Mater Chem A* 2017;5:19836-45. DOI
78. Tan L, Jiang Z, Gao Y, Zhang S. Synergistic interaction between *in situ* exsolved and phosphorized nanoparticles and perovskite oxides for enhanced electrochemical water splitting. *Int J Hydrogen Energy* 2022;47:20016-26. DOI
79. Shang C, Xiao X, Xu Q. Coordination chemistry in modulating electronic structures of perovskite-type oxide nanocrystals for oxygen evolution catalysis. *Coord Chem Rev* 2023;485:215109. DOI
80. Kim BJ, Fabbri E, Abbott DF, et al. Functional role of Fe-doping in Co-based perovskite oxide catalysts for oxygen evolution reaction. *J Am Chem Soc* 2019;141:5231-40. DOI
81. Deng H, Feng C, Zhang W, et al. The electrolyte-layer free fuel cell using a semiconductor-ionic $Sr_2Fe_{1.5}Mo_{0.5}O_{6-\delta}$ - $Ce_{0.8}Sm_{0.2}O_{2-\delta}$ composite functional membrane. *Int J Hydrogen Energy* 2017;42:25001-7. DOI
82. Rath MK, Lee K. Superior electrochemical performance of non-precious Co-Ni-Mo alloy catalyst-impregnated $Sr_2FeMoO_{6-\delta}$ as an electrode material for symmetric solid oxide fuel cells. *Electrochim Acta* 2016;212:678-85. DOI
83. Wang W, Li H, Regalado Vera CY, et al. Improving the performance for direct electrolysis of CO_2 in solid oxide electrolysis cells with a $Sr_{1.9}Fe_{1.5}Mo_{0.5}O_{6-\delta}$ electrode *via* infiltration of Pr_6O_{11} nanoparticles. *J Mater Chem A* 2023;11:9039-48. DOI
84. Zhang L, Xu C, Sun W, et al. Constructing perovskite/alkaline-earth metal composite heterostructure by infiltration to revitalize CO_2 electrolysis. *Sep Purif Technol* 2022;298:121475. DOI
85. Yu W, Zhang D, Zhang X, Liu T, Wang Y. Advanced Ru-infiltrated perovskite oxide electrodes for boosting the performance of syngas fueled solid oxide fuel cell. *ChemElectroChem* 2022;9:e202200024. DOI
86. Osinkin D, Beresnev S, Bogdanovich N. Influence of Pr_6O_{11} on oxygen electroreduction kinetics and electrochemical performance of $Sr_2Fe_{1.5}Mo_{0.5}O_{6-\delta}$ based cathode. *J Power Sources* 2018;392:41-7. DOI
87. Li M, Hou J, Fan Y, Xi X, Fu X, Luo J. Interface modification of Ru-CeO_2 co-infiltrated SFM electrode and construction of SDC/YSZ bilayer electrolyte for direct CO_2 electrolysis. *Electrochim Acta* 2022;426:140771. DOI

88. Ji Q, Bi L, Zhang J, Cao H, Zhao XS. The role of oxygen vacancies of ABO_3 perovskite oxides in the oxygen reduction reaction. *Energy Environ Sci* 2020;13:1408-28. DOI
89. Hwang J, Rao RR, Giordano L, Katayama Y, Yu Y, Shao-Horn Y. Perovskites in catalysis and electrocatalysis. *Science* 2017;358:751-6. DOI PubMed
90. Mahato N, Banerjee A, Gupta A, Omar S, Balani K. Progress in material selection for solid oxide fuel cell technology: a review. *Prog Mater Sci* 2015;72:141-337. DOI
91. Gao Z, Mogni LV, Miller EC, Railsback JG, Barnett SA. A perspective on low-temperature solid oxide fuel cells. *Energy Environ Sci* 2016;9:1602-44. DOI
92. Myung JH, Neagu D, Miller DN, Irvine JT. Switching on electrocatalytic activity in solid oxide cells. *Nature* 2016;537:528-31. DOI PubMed
93. Liu S, Liu Q, Fu X, Luo J. Cogeneration of ethylene and energy in protonic fuel cell with an efficient and stable anode anchored with *in-situ* exsolved functional metal nanoparticles. *Appl Catal B Environ* 2018;220:283-9. DOI
94. Neagu D, Oh TS, Miller DN, et al. Nano-socketed nickel particles with enhanced coking resistance grown *in situ* by redox exsolution. *Nat Commun* 2015;6:8120. DOI PubMed PMC
95. Calì E, Thomas MP, Vasudevan R, et al. Real-time insight into the multistage mechanism of nanoparticle exsolution from a perovskite host surface. *Nat Commun* 2023;14:1754. DOI PubMed PMC
96. Zhang S, Jiang Y, Han H, Li Y, Xia C. Perovskite oxyfluoride ceramic with in situ exsolved Ni-Fe nanoparticles for direct CO_2 electrolysis in solid oxide electrolysis cells. *ACS Appl Mater Interfaces* 2022;14:28854-64. DOI
97. Hu Y, Han H, Hu H, et al. Potassium doping effects on the structure and magnetic properties of Sr_2FeMoO_6. *J Alloys Compd* 2012;526:1-5. DOI
98. Yang X, Chen J, Panthi D, et al. Electron doping of $Sr_2FeMoO_{6-\delta}$ as high performance anode materials for solid oxide fuel cells. *J Mater Chem A* 2019;7:733-43. DOI
99. Azizi F, Kahoul A, Azizi A. Effect of La doping on the electrochemical activity of double perovskite oxide Sr_2FeMoO_6 in alkaline medium. *J Alloys Compd* 2009;484:555-60. DOI
100. Neagu D, Tsekouras G, Miller DN, Ménard H, Irvine JT. In situ growth of nanoparticles through control of non-stoichiometry. *Nat Chem* 2013;5:916-23. DOI PubMed
101. Mccolm TD, Irvine JTS. B site doped strontium titanate as a potential SOFC substrate. *Ionics* 2001;7:116-21. DOI
102. Sun Y, Li J, Zeng Y, et al. A-site deficient perovskite: the parent for *in situ* exsolution of highly active, regenerable nano-particles as SOFC anodes. *J Mater Chem A* 2015;3:11048-56. DOI
103. Yang G, Feng J, Sun W, et al. The characteristic of strontium-site deficient perovskites $Srx Fe_{1.5}Mo_{0.5}O_{6-\delta}$ (x = 1.9-2.0) as intermediate-temperature solid oxide fuel cell cathodes. *J Power Sources* 2014;268:771-7. DOI
104. Feng J, Qiao J, Wang W, Wang Z, Sun W, Sun K. Development and performance of anode material based on A-site deficient $Sr_{2-x}Fe_{1.4}Ni_{0.1}Mo_{0.5}O_{6-\delta}$ perovskites for solid oxide fuel cells. *Electrochim Acta* 2016;215:592-9. DOI
105. Tan T, Wang Z, Huang K, Yang C. High-performance co-production of electricity and light olefins enabled by exsolved NiFe alloy nanoparticles from a double-perovskite oxide anode in solid oxide-ion-conducting fuel cells. *ACS Nano* 2023;17:13985-96. DOI PubMed
106. Wang Z, Tan T, Du K, Zhang Q, Liu M, Yang C. A high-entropy layered perovskite coated with in situ exsolved core-shell CuFe@FeO*x* nanoparticles for efficient CO_2 electrolysis. *Adv Mater* 2023;36:2312119. DOI PubMed
107. Xiao G, Liu Q, Dong X, Huang K, Chen F. $Sr_2Fe_{4/3}Mo_{2/3}O_6$ as anodes for solid oxide fuel cells. *J Power Sources* 2010;195:8071-4. DOI
108. Lv H, Lin L, Zhang X, et al. *In situ* exsolved $FeNi_3$ nanoparticles on nickel doped $Sr_2Fe_{1.5}Mo_{0.5}O_{6-\delta}$ perovskite for efficient electrochemical CO_2 reduction reaction. *J Mater Chem A* 2019;7:11967-75. DOI
109. Qiu P, Yang X, Wang W, et al. Redox-reversible electrode material for direct hydrocarbon solid oxide fuel cells. *ACS Appl Mater Interfaces* 2020;12:13988-95. DOI
110. He F, Hou M, Zhu F, et al. Building efficient and durable hetero-interfaces on a perovskite-based electrode for electrochemical CO_2 reduction. *Adv Energy Mater* 2022;12:2202175. DOI
111. Muñoz-García AB, Bugaris DE, Pavone M, et al. Unveiling structure-property relationships in $Sr_2Fe_{1.5}Mo_{0.5}O_{6-\delta}$, an electrode material for symmetric solid oxide fuel cells. *J Am Chem Soc* 2012;134:6826-33. DOI
112. Ye L, Zhang M, Huang P, et al. Enhancing CO_2 electrolysis through synergistic control of non-stoichiometry and doping to tune cathode surface structures. *Nat Commun* 2017;8:14785. DOI PubMed PMC
113. Sun YF, Zhang YQ, Chen J, et al. New opportunity for *in situ* exsolution of metallic nanoparticles on perovskite parent. *Nano Lett* 2016;16:5303-9. DOI PubMed
114. Yang Y, Li J, Sun Y. The metal/oxide heterointerface delivered by solid-based exsolution strategy: a review. *Chem Eng J* 2022;440:135868. DOI
115. Liu S, Liu Q, Luo JL. Highly stable and efficient catalyst with in situ exsolved Fe-Ni alloy nanospheres socketed on an oxygen deficient perovskite for direct CO_2 electrolysis. *ACS Catal* 2016;6:6219-28. DOI
116. Tsvetkov N, Lu Q, Sun L, Crumlin EJ, Yildiz B. Improved chemical and electrochemical stability of perovskite oxides with less reducible cations at the surface. *Nat Mater* 2016;15:1010-6. DOI PubMed
117. Song Y, Min J, Guo Y, et al. Surface activation by single Ru atoms for enhanced high-temperature CO_2 electrolysis. *Angew Chem*

Int Ed Engl 2024;63:e202313361. DOI PubMed

118. Kim YH, Jeong H, Won BR, Myung JH. Exsolution modeling and control to improve the catalytic activity of nanostructured electrodes. *Adv Mater* 2023;35:e2208984. DOI
119. Gu J, Hsu CS, Bai L, Chen HM, Hu X. Atomically dispersed Fe^{3+} sites catalyze efficient CO_2 electroreduction to CO. *Science* 2019;364:1091-4. DOI PubMed
120. Lv H, Lin L, Zhang X, et al. In situ investigation of reversible exsolution/dissolution of CoFe alloy nanoparticles in a Co-doped $Sr_2Fe_{1.5}Mo_{0.5}O_{6-\delta}$ cathode for CO_2 electrolysis. *Adv Mater* 2020;32:e1906193. DOI PubMed
121. Lv H, Lin L, Zhang X, et al. Promoting exsolution of RuFe alloy nanoparticles on $Sr_2Fe_{1.4}Ru_{0.1}Mo_{0.5}O_{6-\delta}$ via repeated redox manipulations for CO_2 electrolysis. *Nat Commun* 2021;12:5665. DOI PubMed PMC
122. Weber ML, Wilhelm M, Jin L, et al. Exsolution of embedded nanoparticles in defect engineered perovskite layers. *ACS Nano* 2021;15:4546-60. DOI PubMed
123. Opitz AK, Nenning A, Vonk V, et al. Understanding electrochemical switchability of perovskite-type exsolution catalysts. *Nat Commun* 2020;11:4801. DOI PubMed PMC
124. Zhang BW, Zhu MN, Gao MR, et al. Boosting the stability of perovskites with exsolved nanoparticles by B-site supplement mechanism. *Nat Commun* 2022;13:4618. DOI PubMed PMC
125. Zhang BW, Zhu MN, Gao MR, et al. Phase transition engineering of host perovskite toward optimal exsolution-facilitated catalysts for carbon dioxide electrolysis. *Angew Chem Int Ed Engl* 2023;62:e202305552. DOI PubMed
126. Hong J, Heo SJ, Singh P. Water mediated growth of oriented single crystalline $SrCO_3$ nanorod arrays on strontium compounds. *Sci Rep* 2021;11:3368. DOI PubMed PMC
127. Fu G, Kang X, Zhang Y, et al. Capturing critical gem-diol intermediates and hydride transfer for anodic hydrogen production from 5-hydroxymethylfurfural. *Nat Commun* 2023;14:8395. DOI PubMed PMC
128. Sun Z, Lin L, He J, et al. Regulating the spin state of Fe^{III} enhances the magnetic effect of the molecular catalysis mechanism. *J Am Chem Soc* 2022;144:8204-13. DOI PubMed
129. Liu J, Luo W, Wang L, Zhang J, Fu X, Luo J. Toward excellence of electrocatalyst design by emerging descriptor-oriented machine learning. *Adv Funct Mater* 2022;32:2110748. DOI
130. Li J, Yu Y, Xu S, Yan W, Mu S, Zhang JN. Function of electron spin effect in electrocatalysts. 2023. Available from: https://www.whxb.pku.edu.cn/EN/10.3866/PKU.WHXB202302049. [Last accessed on 21 Feb 2024].
131. He ZD, Tesch R, Eslamibidgoli MJ, Eikerling MH, Kowalski PM. Low-spin state of Fe in Fe-doped NiOOH electrocatalysts. *Nat Commun* 2023;14:3498. DOI PubMed PMC
132. Chen A, Zhang X, Zhou Z. Machine learning: accelerating materials development for energy storage and conversion. *InfoMat* 2020;2:553-76. DOI
133. Zhai S, Xie H, Cui P, et al. A combined ionic Lewis acid descriptor and machine-learning approach to prediction of efficient oxygen reduction electrodes for ceramic fuel cells. *Nat Energy* 2022;7:866-75. DOI